Characteristics of "third family" compact stars

Eigenschaften von kompakten Objekten der dritten Generation
Bachelor-Thesis von Matthias Manfred Seubert
Tag der Einreichung:

1. Gutachten: Priv.-Doz. Dr. M. Buballa
2. Gutachten: Prof. Dr. G. Moore

TECHNISCHE
UNIVERSITÄT
DARMSTADT

Fachbereich Physik
Institut für Kernphysik

Characteristics of "third family" compact stars
Eigenschaften von kompakten Objekten der dritten Generation

Vorgelegte Bachelor-Thesis von Matthias Manfred Seubert

1. Gutachten: Priv.-Doz. Dr. M. Buballa
2. Gutachten: Prof. Dr. G. Moore

Tag der Einreichung:

Erklärung zur Bachelor-Thesis

Hiermit versichere ich, die vorliegende Bachelor-Thesis ohne Hilfe Dritter nur mit den angegebenen Quellen und Hilfsmitteln angefertigt zu haben. Alle Stellen, die aus Quellen entnommen wurden, sind als solche kenntlich gemacht. Diese Arbeit hat in gleicher oder ähnlicher Form noch keiner Prüfungsbehörde vorgelegen.

Darmstadt, den 21.04.2017

_____

(Matthias Manfred Seubert)

Abstract

In this work the Tolman-Oppenheimer-Volkoff equations are used to calculate mass-radius relations of neutron stars. We consider different equations of state and assume a phase transition to the deconfined quark phase at high densities. For the quark matter a constant speed of sound equation of state is used. A first-order phase transition could lead to a third stable sequence of compact stars. These "third family" stars can exist beside the two known families of compact objects, the white dwarfs and the neutron stars. We will classify the mass-radius relations and analyze the occurrence of "third family" stars according to the phase transition parameters. In this process we will focus on those types which contain "third family" stars. In case of a phase transition at low transition pressure and large energy density discontinuities, "third family" stars can occur. Furthermore, the general observables like mass and radius of "third family" stars will be analyzed. We find out that "third family" stars and neutron stars can have the same mass. These non-identical stars are called "neutron star twins". We analyze the structure of these twins and explain why "neutron star twins" give a possible signature for a phase transition. At last we give up the assumption of a sharp first-order phase transition and calculate the mass-radius relations for an equation of state using a smooth interpolation between the two phases. Therefore, we will investigate the effects of smoothening the equation of state on the occurrence of "third family" stars.

Acknowledgments

Contents

1 Introduction and motivation

Since the discovery of the atomic nucleus in 1911 by Rutherford et al., it is one of the major goals of nuclear physics to explore the properties of matter at nuclear densities and beyond. Hence in the recent years, larger and more expensive facilities were build (like the LHC at CERN or FAIR), to push our experimental knowledge of hot dense matter. In astrophysics, neutron stars provide a unique laboratory to study the structure and interaction of matter at high densities and low temperatures.

Most of the observed neutron stars attain masses of $1.4\,M_\odot$ and have radii of about $10\,\mathrm{km}$ [1]. Due to the large compactness, the gravity binds and compresses matter up to ten times of the nuclear saturation density $n_0 = 0.16\,\mathrm{fm}^{-3}$ [2]. The matter inside a neutron star is described by the equation of state (EoS). Using different approaches to the particle interactions lead to various equations of state (EoSs). The masses of the recently observed pulsars J1614-2230 $(M = (1.97 \pm 0.04)\,M_\odot$ [3]$)$ and J0348+0432 $(M = (2.01 \pm 0.04)\,M_\odot$ [4]$)$ can be reproduced by a sufficiently stiff equation of state ($dP/d\epsilon$ is large). Since cold matter at densities above $\approx 2\,n_0$ can not be reproduced by particle accelerators, there is no direct experimental data for matter at low temperature and high densities to adapt the equation of state. At these densities, the EoS is not known well and there exist various approaches for it.

The strong interactions of matter at high densities is described by the theory of quantum chromodynamics (QCD). However an exact solution for the cold neutron star matter is not possible within QCD. The densities are too low to apply perturbative QCD [5] and lattice QCD is stymied by the numerical sign problem [7]. Nevertheless we will assume a phase transition at densities above n_0 from the confined hadronic matter to the deconfined quark matter with regard to the QCD phase diagram in Figure 1.1. The neutron star matter is found at low temperatures in the hadron phase and maybe overlaps overlaps with the color superconductive quark matter phase. In this region the phase change is assumed to be first-order [8] but the exact matter configurations in compact stars are still unknown [9]. For this reason we will construct both, hybrid EoSs (consisting of a hadronic and quark phase) using a first-order phase transition and

Figure 1.1: Scetch of the QCD phase diagram in the T-μ plane. For low temperatures we distinguish between the hadron/nuclear phase at low μ and the color superconductive phase at high μ. For high temperatures the quark gluon plasma occurs [6].

hadron-quark crossover to interpolate the transition region.

Compact objects like white dwarfs and neutron stars emerge at the end of the stellar evolution. The mass of the dying star is the crucial factor whether a white dwarf, a neutron star or a black hole arises. It is expected that for stars with a maximal mass of $4\,M_\odot$, a white dwarf occurs [11]. White dwarfs have mas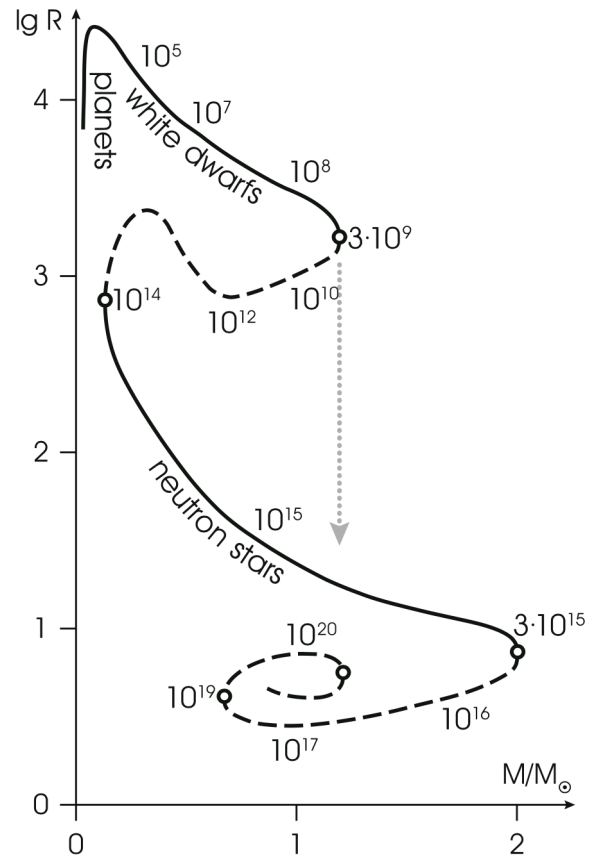ses up to the Chandrasekhar limit of $1.4\,M_\odot$ and are stabilized by the pressure of degenerated electrons [12]. They form one stable sequence of compact objects for large ($R \approx 10^4\,$km) radii [10]. The mass-radius relation for compact objects is shown in Figure 1.2. For higher central densities than $3 \times 10^9\,$g/cm^3, the white dwarf destabilizes and collapses.

The second stable sequence of compact objects occurs at higher densities and lower radii. Neutron stars form this stable branch. The stars are stable due to the nucleon Fermi pressure and the repulsion between nucleons at short range [12]. They originate from stars more massive than $4\,M_\odot$ [11] and destabilize at densities above $3 \times 10^{15}\,$g/cm^3.

Figure 1.2: MR relations of compact objects containing the two stable families white dwarfs and neutron stars. The central density of some characteristic stars is denoted by units of $[\rho_c] = $ g/cm^3 [10].

Nearly 50 years ago Gerlach found out, that a third sequence of stable equilibrium configurations of compact objects at even higher densities is not forbidden by general relativity [13]. Therefore "third family" stars could exist beside the two known families white dwarfs and neutron stars. The necessary condition for their existence is a sufficiently large discontinuity in the speed of sound $c_s^2 = \mathrm{d}P/\mathrm{d}\epsilon$. Wheeler and collaborators [14] demonstrated that for rather smooth EoSs, "third family" stars can not occur. However Glendenning and Kettner [15] found that a first-order phase transition to deconfined quark matter with sufficiently high energy density discontinuity satisfies Gerlach's necessary condition of "third family" stars and can indeed lead to "third family" stars. In this process the deconfinement softens the EoS due to the loss of the repulsion between nucleons at short range. According to the Pauli principle the Fermi pressure is shared among a higher number of quarks, which will further reduce the pressure at a given energy density [12]. This softened EoS will destabilize the star first. At high densities this EoS will somehow lead to a stable star configuration containing a quark matter core.

In this thesis we investigate the necessary conditions of the phase transition to obtain "third family" stars. For this purpose we use different hadronic EoSs and assume a constant speed of sound for the quark matter. Considering a first-order phase transition, we analyze the dependency on mass-radius relations with reference to the transition pressure and the energy density discontinuity. In this process we calculate the range of values of the transition parameters for which stable third branches of compact objects can occur. In dependency on these transition parameters, general properties like the minimal/maximal mass and radius will be discussed. Since the mass regions of "third family" and neutron stars partially overlap, we can find non-identical stars with the same mass. The structure of these "neutron star twins" will be compared and we argue that the observation of such twin stars provides a signature for phase transitions in the interior of neutron stars. In contrast to the work of Glendenning and Kettner, we also construct a smooth transition by a crossover and analyze the changes for mass-radius relations and the occurrence of "third family" stars.

We will structure this thesis as follows:
In Chapter 2 we present the necessary physical and mathematical background to understand neutron stars. First we give a short introduction about the structure of neutron stars. Then the ordinary differential equations, the Tolman-Oppenheimer-Volkoff equations, will be derived from general relativity. These equations describe the equilibrium solutions of the interior of static stars. This gives us the possibility to describe observables like mass and radius in dependency on the EoS and the central pressure. The used equation of state as well as their mass-radius relations will be presented and discussed.

Chapter 3 deals with the mass-radius relations considering a first-order phase transition. At first we summarize characteristics of first-order phase transitions and introduce the constant speed of sound (CSS) parametrization. For a given hadronic and quark EoS, the overall EoS containing a phase transition is determined by two parameters. According to these two parameters we can derive a generic condition for stable hybrid stars. After that we present four possible types of mass-radius relations and visualize the regions of their occurrence in a "phase" diagram as a function of the transition parameters. Two of the four types contain a "third family" branch. For these two regions we will analyze the observables of the "third family" stars. Finally we compare the structure of "neutron star twins" and discuss why their existence gives a possible hint for a phase transition in the interior of a neutron star.

In Chapter 4 we give up the assumption of a sharp phase transition and introduce a smooth interpolation between hadron and quark matter. The consequences of this new equation of state on the mass-radius relations will be investigated. We analyze the occurrence of "third family" stars according to the crossover region which indicates the smoothness of the EoS. Therefore we can see how smooth an EoS can be to satisfy the necessary condition of Gerlach.

In the last Chapter we summarize the results and provide an outlook for further research.

2 Neutron stars, general relativity and the equation of state

In this chapter we discuss the physical background of this thesis. First of all we concentrate on neutron stars in general. We will discuss their structure and the theoretical framework which is necessary to compute this structure. This section is used to establish the Tolman-Oppenheimer-Volkoff equations, which give us the possibility to describe neutron stars in dependence of the central pressure and the equation of state. Finally we present different equations of state and their influence on observables like mass and radius of neutron stars.

2.1 Neutron stars in general

At the end of the evolution of stars more massive than $(5-8)\,M_\odot$, their cores undergo a gravitational collapse, during which their outer pre-supernova layers, are blown away in a shockwave [11]. A compact star called neutron star (NS) remains which is in hydrostatical equilibrium between Fermi pressure, the repulsion between nucleons at short range and the gravitational attraction. These superdense objects have masses of $(1-2)\,M_\odot$ at radii about $R \approx 10\,\mathrm{km}$. This leads to an average mass density $\rho \approx 7 \times 10^{14}\,\mathrm{g\ cm^{-3}} = (2-3)\,\rho_0$, where $\rho_0 = 2.8 \times 10^{14}\,\mathrm{g\ cm^{-3}}$ denotes the nuclear density [2]. In the center the density is even larger, reaching up to $10\,\rho_0$ [9]. The perinatal temperature is very high ($T > 10^{10}\,\mathrm{K}$) but drops rapidly due to neutrino emission. A month after the collapse the temperature fell to $T \approx 10^8\,\mathrm{K}$ ($k_B T \approx 10\,\mathrm{keV}$) [10], which can be considered as cold compared to the high energy densities in the interior of the star. Therefore we will consider cold ($T = 0$) neutron stars in this work. For properties like mass and radius this assumption is even justifiable in the crust [12].

2.1.1 Structure of neutron stars

Towards current theories a neutron star can be divided into 5 regions, the atmosphere, the envelope, the crust, the outer and inner core. These regions are shown in Figure 2.1 and differ in thickness, mass density and internal structure. The core of NSs holds up to 99% of the mass.

The **atmosphere** differs in thickness from a few millimetres (in cold NSs) up to centimetres (in hot NSs) and has wide influence on the emitted radiation. Out of the spectrum of radiation we can get useful information about the radius or mass. The atmosphere is still not fully understood. The surface can even be liquid or solid in very cold or ultramagnetized NSs [2].

The release of thermal energy to the surface is influenced by the **envelope** [17]. It consists of ions and electrons and is a couple of hundred metres thick. The electrons produce the principle part of the pressure in this region. This pressure fully ionize the atoms. Near the atmosphere there exists a non-degenerate electron gas which becomes degenerated, nearly ideal and ultra-
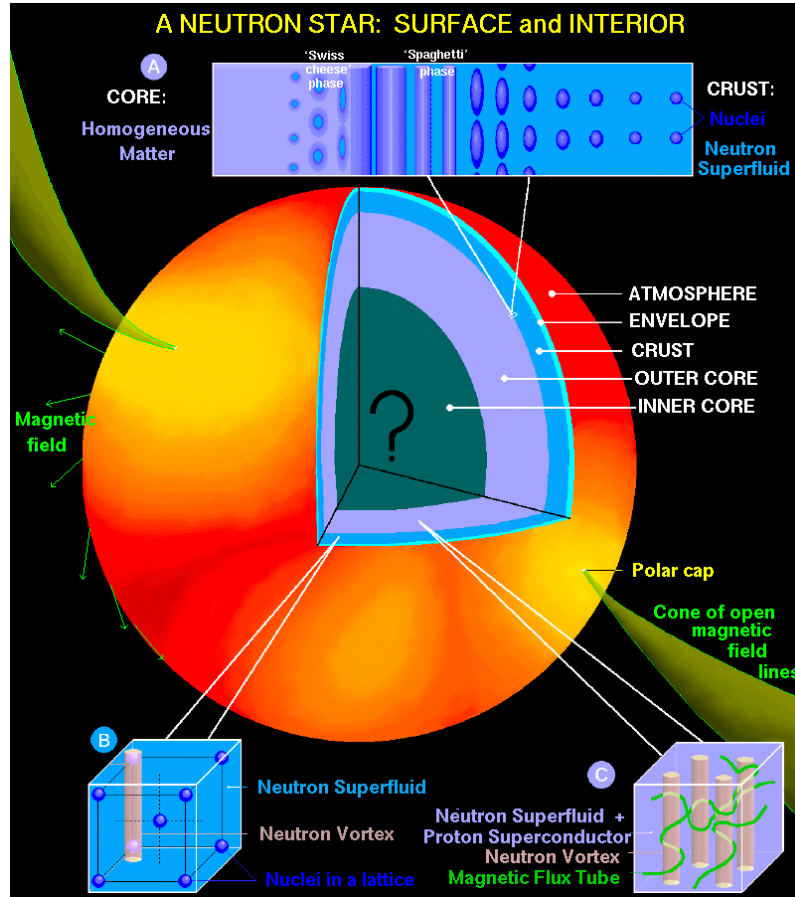
Figure 2.1: The structure of a neutron stars with the five pictured regions: the atmosphere, the envelope, the crust and the outer/inner core [16].

relativistic in deeper layers with a density of $\rho \approx 10^6\,\mathrm{g\,cm^{-3}}$ [2].

Extending to a depth of 1-2 kilometres, the **crust** contains especially nuclei. The nuclei range from ^{56}Fe at layers next to the envelope, to nuclei with A $\approx$ 200 at mass densities of $\rho \approx (0.3 - 0.5)\,\rho_0$ near the core-crust interface [17]. Since the electron Fermi energy increases with rising densities ρ, the electron capture is elicited. Therefore neutron rich nuclei appear. At a density of $\rho_{\mathrm{dr}} \approx 4.3 \times 10^{11}\,\mathrm{g\,cm^{-3}}$ the neutron drip is reached. This determines the point where the binding energy of neutrons inside nuclei is zero. The neutrons start to escape the nuclei and produce a free neutron gas [10] between the lattice ions.

The **outer core** is a few kilometres thick and the density ranges from $0.5\rho_0$ to $2\rho_0$. The matter is in a npeμ composition, which means that the matter consists mainly of neutrons alongside with small percentages of protons, electrons and muons [2]. All particles are strongly degenerated and their concentrations range due to the electrical neutrality [12] and the equilibrium of β-decay (n $\rightleftharpoons$ p$^+$ + e$^-$ + $\overline{\nu}_e$). The neutrinos are not taken into cosideration as they will leave the star directly [10].

Only in high-mass stars the fifth region occurs: the **inner core**. The densities rise up from $2\rho_0$ to the central density of $10\,\rho_0$ within a few kilometres. There are different theories and models about the matter configuration in this region like hyperonizaton, pion or kaon condensation and

a phase transition to a deconfined phase of quark matter. In this thesis we will focus on the last hypothesis. Stars in which the hadrons are converted to quark matter due to high pressure are called hybrid stars [12, 2].

2.2 General relativity

Einstein's theory of gravitation and spacetime, general relativity (GR), was published and introduced in three papers in 1915 [18, 19, 20]. This theory is the foundation of our understanding of dense objects like neutron stars. These objects could also be described in Newton's theory of gravity, but they would have very different characteristics. Goal of this section is a derivation of the Tolman-Oppenheimer-Volkoff (TOV) equations which describe the structure of relativistic stars. A deeper understanding and further information about GR can be obtained by [21]. In this thesis we will use the same notations and statements to derive the TOV equations as used in [21]. The metric signature of [21] (+,-,-,-) and the Einstein notation is used. We sum over contracted indices [22].

2.2.1 Fundamental principles, mathematics and expressions

General relativity is based on three essential principles:

Out of the special relativity (SR) we can deduce a **generalized principle of relativity**. This means that not only in every inertial reference system (IS) the physical laws are valid in the same way but also in accelerated frames of reference.
A further physical base for the GR is the **equivalence principle**. In conclusion this principle deals with the equivalence between gravitational and inertial forces. Therefore gravitational and inertial mass must be the same. Einstein generalized this principle in the way that in all sufficiently small free falling reference frames (local IS) everything behaves as if there is no gravitational force at all.
Based on the equivalence principle we can define the **principle of covariance**. With this principle we can derive physical laws containing gravitational effects out of general laws of the special relativity. The valid equations in a gravitational field must satisfy the following conditions: The equations are covariant under general transformation of coordinates and valid for a local inertial system (all laws are equal to the ones of special relativity if the metric tensor is equal to the Minkowski tensor).

General relativity is defined on a four dimensional Riemannian manifold. Coordinates in this non-Euclidian space are denoted by $x^\mu = (x^0, x^1, x^2, x^3)$. ξ^α denotes a flat tangential space wherein the laws of SR hold. The indices $\mu, \nu, \lambda, ..$ describe coordinates of the Riemannian space, $\alpha, \beta, \gamma, ...$ coordinates of the Minkowski space. For every point in the Riemannian manifold exists a coordinate transformation $\mathbf{x}^\mu = \mathbf{x}^\mu(\xi)$ and it holds the connection between Lorentz vector $d\xi^\alpha$ and Riemann vector dx^μ

$$dx^\mu = \frac{\partial x^\mu}{\partial \xi^\alpha} d\xi^\alpha. \tag{2.1}$$

Therefore we can rewrite the invariant line element ds^2 in the following way

$$ds^2 = \eta_{\alpha\beta}d\xi^\alpha d\xi^\beta = g_{\mu\nu}(x)\,dx^\mu dx^\nu, \qquad \text{with} \qquad g_{\mu\nu}(x) = \eta_{\alpha\beta}\frac{\partial\xi^\alpha}{\partial x^\mu}\frac{\partial\xi^\beta}{\partial x^\nu}. \qquad (2.2)$$

In contrast to the Minkowski tensor $\eta_{\alpha\beta}$ in SR, the metric tensor $g_{\mu\nu}$ of GR depends on the four dimensional space-time. Analogously to Equation (2.2), we can define a Riemann vector $A^\mu \equiv \partial x^\mu / \partial\xi^\alpha A^\alpha$ by the Lorentz vector A^α. The metric tensor can be used to transform any contravariant Riemann vector to its covariant counterpart and vice versa

$$A_\mu = g_{\mu\nu}A^\nu, \qquad A^\mu = g^{\mu\nu}A_\nu, \qquad (2.3)$$

where $g^{\mu\nu}$ is the inverse of the metric tensor $g_{\mu\nu}$.

In the following we will concentrate on the equation of motion. A force-free mass point in a local inertial system will move according to the following equation

$$\frac{d^2\xi^\alpha}{d\tau^2} = c^2\frac{d^2\xi^\alpha}{ds^2} = 0, \qquad (2.4)$$

with the proper time τ and velocity of light in vacuum c. According to the thoughts above (Equation (2.3)), we can rewrite the equation of motion in a way that it describes particles in gravitational fields

$$0 = \frac{d}{d\tau}\left(\frac{\partial\xi^\alpha}{\partial x^\mu}\frac{dx^\mu}{d\tau}\right) = \frac{d^2x^\kappa}{d\tau^2} - \Gamma^\kappa_{\mu\nu}\frac{dx^\mu}{d\tau}\frac{dx^\nu}{d\tau}. \qquad (2.5)$$

In Equation (2.5) we use the identity $\frac{\partial\xi^\alpha}{\partial x^\mu}\frac{\partial x^\kappa}{\partial\xi^\alpha} = \delta^\kappa_\mu$ and introduce the Christoffel symbol $\Gamma^\kappa_{\mu\nu}$. The path of a particle described by Equation (2.5) is called geodetic line and is a straight line in case of the Minkowski metric. Expressing the Christoffel symbol by the metric tensor, we obtain

$$\Gamma^\kappa_{\lambda\mu} = \frac{g^{\kappa\nu}}{2}\left(\frac{\partial g_{\mu\nu}}{\partial x^\lambda} + \frac{\partial g_{\lambda\nu}}{\partial x^\mu} - \frac{\partial g_{\mu\lambda}}{\partial x^\nu}\right). \qquad (2.6)$$

Now we are introducing the following compact notations for the covariant derivatives of a covariant and contravariant tensor

$$A^\mu_{\,\|\nu} \equiv A^\mu_{\,|\nu} + \Gamma^\mu_{\nu\lambda}A^\lambda, \qquad \text{with the partial derivatives} \qquad A^\mu_{\,|\nu} \equiv \frac{\partial A^\mu}{\partial x^\nu}.$$

$$A_{\mu\|\nu} \equiv A_{\mu|\nu} + \Gamma^\lambda_{\mu\nu}A_\lambda, \qquad\qquad\qquad A_{\mu|\nu} \equiv \frac{\partial A_\mu}{\partial x^\nu}. \qquad (2.7)$$

Since the metric coefficients $g_{\mu\nu}(x)$ describe a curved space, we will analyze this curvature quantitatively by the **Riemann curvature tensor** $R_{\kappa\nu\mu\lambda}$, which can be derived from the equations above. If the curvature tensor vanishes, the space will be flat. From this tensor we can obtain the Ricci tensor $R_{\mu\lambda}$ and the scalar curvature R by contraction

$$R_{\kappa\nu\mu\lambda} = \frac{1}{2}\left(\frac{\partial^2 g_{\kappa\nu}}{\partial x^\mu\partial x^\lambda} + \frac{\partial^2 g_{\mu\lambda}}{\partial x^\kappa\partial x^\nu} - \frac{\partial^2 g_{\mu\nu}}{\partial x^\kappa\partial x^\lambda} - \frac{\partial^2 g_{\kappa\lambda}}{\partial x^\mu\partial x^\nu}\right) + g_{\zeta\sigma}(\Gamma^\zeta_{\nu\kappa}\Gamma^\sigma_{\mu\lambda} - \Gamma^\zeta_{\lambda\kappa}\Gamma^\sigma_{\mu\nu}), \qquad (2.8)$$

$$R_{\mu\lambda} = g^{\nu\kappa}R_{\nu\mu\kappa\lambda}, \qquad (2.9)$$

$$R = g^{\mu\nu}R_{\mu\nu}. \qquad (2.10)$$

Because of symmetry properties, the Riemann curvature tensor has 20 independent components. Using the definition of the curvature tensor one can derive a fundamental property of it, the second Bianchi identity [21]

$$R_{\mu\nu\lambda\kappa||\sigma} + R_{\mu\nu\kappa\sigma||\lambda} + R_{\mu\nu\sigma\lambda||\kappa} = 0 \,. \tag{2.11}$$

The **Einstein field equations** connect the space time curvature with the energy and momentum in this space time. The energy and momentum in space time is described by the energy-momentum-tensor $T^{\mu\nu}$. For an ideal fluid it has the following form

$$T_{\mu\nu} = \left(\epsilon + \frac{P}{c^2} \right) u_\mu u_\nu - g_{\mu\nu} P \,, \tag{2.12}$$

with the energy density ϵ, the pressure P and the fluid four-velocity $u_\mu = dx_\mu/d\tau$. Since in a local IS there are no gravitational fields, the Einstein field equations can not be derived from the principle of covariance. Therefore we have to determine the equations by preferably easy assumptions, like those that they are covariant and contain the Newtonian limit. Rewriting the second Bianchi identity, we can define the Einstein tensor $G_{\mu\nu}$ and derive the Einstein field equations [21]

$$G_{\mu\nu||\nu} := \left(R_{\mu\nu} - \frac{R}{2} g_{\mu\nu} \right)_{||\nu} = 0 \,, \tag{2.13}$$

$$R_{\mu\nu} - \frac{R}{2} g_{\mu\nu} = -\frac{8\pi G}{c^4} T_{\mu\nu} \quad \Leftrightarrow \quad R_{\mu\nu} = -\frac{8\pi G}{c^4} \left(T_{\mu\nu} - \frac{T}{2} g_{\mu\nu} \right), \tag{2.14}$$

where G denotes the gravitational constant and T the trace of $T_{\mu\nu}$. Since $R_{\mu\nu}$, $g_{\mu\nu}$ and $T_{\mu\nu}$ are symmetric, the Einstein field equations contain ten independent components. By using the two equations (2.13) and (2.14) above, we get a form of energy conservation $T_{\mu\nu||\nu} = 0$.

2.2.2 Metric in static isotropic spacetime

Since the field equations are not linear, there is no standard method to solve them. For an exact analytic solution we have to make simplifying assumptions. In this section we will assume an isotropic and static spacetime. For this we will use a standard form and calculate the components of the Ricci tensor. When the distance r from the observed object goes to infinity, the metric must behave like the Minkowski metric. r, θ and ϕ denote spherical coordinates and t the time coordinate. The line element of static isotropic space time may be expressed as

$$ds^2 = g_{\mu\nu} dx^\mu dx^\nu = B(r)c^2 dt^2 - A(r) dr^2 - r^2 (d\theta^2 + \sin^2\theta d\phi^2) \,. \tag{2.15}$$

To satisfy the limit of the Minkowski metric for $r \to \infty$, A(r) and B(r) must fulfill

$$\lim_{r\to\infty} A(r) = 1, \qquad\qquad \lim_{r\to\infty} B(r) = 1 \,. \tag{2.16}$$

The line element (2.15) has a corresponding metric

$$g_{\mu\nu} = \mathrm{diag}(B(r), -A(r), -r^2, -r^2 \sin^2\theta) \,. \tag{2.17}$$

With this metric we obtain the Ricci tensor with the following components[1]

$$R_{00} = -\frac{B''}{2A} + \frac{B'}{4A}\left(\frac{A'}{A} + \frac{B'}{B}\right) - \frac{B'}{rA}, \qquad R_{33} = R_{22}\sin^2\theta,$$

$$R_{11} = \frac{B''}{2B} - \frac{B'}{4B}\left(\frac{A'}{A} + \frac{B'}{B}\right) - \frac{A'}{rA}, \qquad R_{\mu\nu} = 0 \text{ for } \mu \neq \nu, \qquad (2.18)$$

$$R_{22} = -1 - \frac{r}{2A}\left(\frac{A'}{A} - \frac{B'}{B}\right) + \frac{1}{A}.$$

2.2.3 The Tolman-Oppenheimer-Volkoff equations

The Tolman-Oppenheimer-Volkoff (TOV) equations are the solutions of the Einstein field equations inside a spherical, static star containing an ideal fluid. For a static problem ($u^i(x) = 0$ for $i = 1, 2, 3$) holds

$$c^2 = g_{\mu\nu}u^\mu u^\nu = g_{00}(u^0)^2 \qquad \Leftrightarrow \qquad u^0 = \frac{c}{\sqrt{B}} \qquad \text{and} \qquad u_0 = c\sqrt{B}. \qquad (2.19)$$

Hence we can rewrite the general energy momentum tensor (2.12)

$$T_{\mu\nu} = \text{diag}(\epsilon c^2 B,\ PA,\ Pr^2,\ Pr^2\sin^2\theta). \qquad (2.20)$$

With the inverse of the metric tensor $g_{\mu\nu}$ we can compute the trace of the energy momentum tensor: $T = g^{\mu\nu}T_{\mu\nu} = \epsilon c^2 - 3P$. With the results above and the Einstein field equations we can relate the components of the Ricci tensor to our source terms

$$R_{00} = -\frac{4\pi G}{c^4}(\epsilon c^2 + 3P)B, \quad R_{11} = -\frac{4\pi G}{c^4}(\epsilon c^2 - P)A, \quad R_{22} = -\frac{4\pi G}{c^4}(\epsilon c^2 - P)r^2. \quad (2.21)$$

From this we get

$$\frac{R_{00}}{2B} + \frac{R_{11}}{2A} + \frac{R_{22}}{r^2} = -\frac{A'}{rA^2} - \frac{1}{r} + \frac{1}{r^2 A} = -\frac{8\pi G}{c^2}\epsilon \qquad \Leftrightarrow \qquad \frac{d}{dr}\frac{r}{A(r)} = 1 - \frac{8\pi G}{c^2}\epsilon r^2. \qquad (2.22)$$

If we integrate Equation (2.22) from the centre of the star $r = 0$ to the radius r with the additional condition $(r/A)|_{r=0} = 0$ (A must be finite at $r = 0$ because of a continuous mass distribution) we obtain

$$A(r) = \left(1 - \frac{2GM}{c^2 r}\right)^{-1}, \qquad \text{with} \qquad M(r) = 4\pi \int_0^r dr' r'^2 \epsilon(r'). \qquad (2.23)$$

Here, $M(R_{NS})$ denotes the mass of the star with radius R_{NS}. We will now use a property of the Einstein field equations $T^{\mu\nu}_{\|\nu} = 0$. Thus with $\mu = 1$ and the energy momentum tensor $T^{\mu\nu}$ of Equation (2.20) it yields

$$T^{1\nu}_{\|\nu} = \frac{B'}{2A}\left(\epsilon + \frac{P}{c^2}\right)\frac{c^2}{B} + \frac{P'}{A} = 0. \qquad (2.24)$$

---

[1] For clarity we use the following abbreviations: $X = X(r)$, $X' = dX/dr$ and $X'' = d^2X/dr^2$ for $X = A, B$.

Applying (2.24), (2.22) and (2.23) to (2.21), we obtain the Tolman-Oppenheimer-Volkoff equation

$$\frac{dP(r)}{dr} = -\frac{G\,M(r)\,\epsilon(r)}{r^2}\left(1 + \frac{P}{\epsilon(r)\,c^2}\right)\left(1 + \frac{4\pi\,r^3\,P}{M(r)\,c^2}\right)\left(1 - \frac{2\,G\,M(r)}{c^2\,r}\right)^{-1}. \tag{2.25}$$

This equation was first found by Oppenheimer, Tolman and Volkoff [23, 24] in 1939 and describes the relativistic equilibrium between pressure and gravity for a spherical and static star. In the Newtonian limit ($c \to \infty$) we get the equation of the Newtonian hydrostatic equilibrium

$$\frac{dP(r)}{dr} = -\frac{G\,M(r)\,\epsilon(r)}{r^2\,c^2} = -\frac{G\,M(r)\,\rho(r)}{r^2}, \tag{2.26}$$

with the non relativistic mass density ρ.

2.3 Solving the Tolman-Oppenheimer-Volkoff equations

In Section 2.2 we derived the TOV equation and the ordinary differential equation for the mass M

$$\frac{dP(r)}{dr} = -\frac{G\,M(r)\,\epsilon(r)}{r^2}\left(1 + \frac{P}{\epsilon(r)\,c^2}\right)\left(1 + \frac{4\pi\,r^3\,P}{M(r)\,c^2}\right)\left(1 - \frac{2\,G\,M(r)}{c^2\,r}\right)^{-1} \tag{2.27}$$

$$\frac{dM(r)}{dr} = 4\pi\,r^2\,\epsilon(P). \tag{2.28}$$

To solve these equations and get the pressure P(r) and the mass M(r) as a function of the radius r, we have to integrate them from the centre of the neutron star to the distance r. As initial conditions for the integration, we can use that the radius and mass vanish at the centre and the pressure reaches its maximum $P_c := P(r = 0)$. To obtain the overall mass M_{NS} and radius R_{NS} we have to integrate to the surface of the star. With increasing r the pressure will decrease until the surface is reached where the pressure is zero $P(R_{NS}) = 0$. This leads to the definition of R_{NS} and M_{NS}. Figure 2.2 shows the pressure as a function of the radius r. The domain of the integration is not known exactly, which presents a challenge during numerical integration to find the exact radius R_{NS} with $P(R_{NS}) = 0$. This produces large uncertainties for R_{NS}.

To get a consistent domain for all calculations, we rewrite Equation (2.27) and (2.28) by defining $y(P) := r^2$ and use the chain rule $\frac{dM(P)}{dP} = \frac{dM(r)}{dr}\left(\frac{dP(r)}{dr}\right)^{-1}$

$$\frac{dy(P)}{dP} = -\frac{2\,y(P)\,c^2}{G}\frac{(\sqrt{y(P)} - 2\,G\,M(P)/c^2)}{(c^2\,\epsilon(P) + P)(M(P) + 4\pi\,y^{3/2}\frac{P}{c^2})} \tag{2.29}$$

$$\frac{dM(P)}{dP} = -\frac{4\pi\,y^2\,\epsilon(P)}{G}\frac{(\sqrt{y} - 2\frac{M(P)\,G}{c^2})}{(\epsilon(P)\,c^2 + P)(M(P) + 4\pi\,y^{3/2}\frac{P}{c^2})}. \tag{2.30}$$

Equations (2.29) and (2.30) will be integrated over P from the centre P_c to the surface $P_s = 0$.

(a) Pressure P(r) (b) Squared radius y(P)
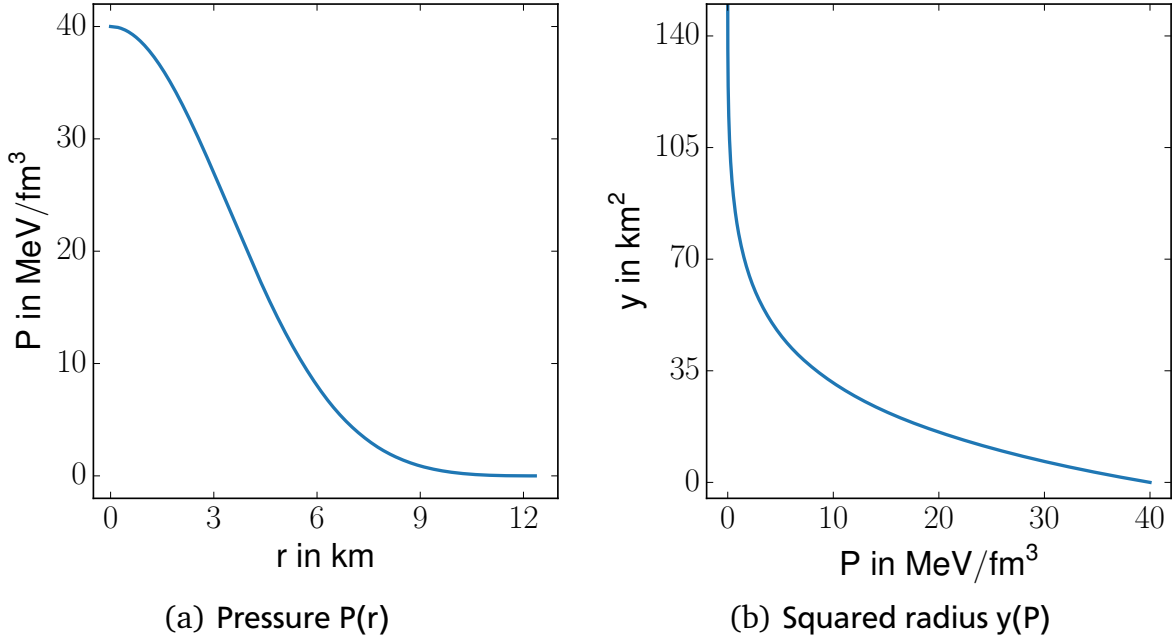
Figure 2.2: The solutions of the pressure P(r) (a) and the squared radius y(P) (b) of the TOV equation for an ideal neutron gas with $P_c = 40\,\mathrm{MeV\,fm^{-3}}$.

2.3.1 Geometrized units

For simplification and clarity it is convenient to use a geometrized unit system with $c = G = 1$, in which we can express the units of all dimensionful quantities in powers of kilometres. For this purpose it holds

$$[\epsilon]_{\mathrm{GU}} = [\epsilon] \cdot \frac{G}{c^4} = 1\,\frac{\mathrm{MeV}}{\mathrm{fm}^3}\frac{G}{c^4} \approx 1.323 \times 10^{-6}\,\mathrm{km^{-2}}$$

$$[P]_{\mathrm{GU}} = [P]_{\mathrm{SI}} \cdot \frac{G}{c^4} = 1\,\frac{\mathrm{kg}}{\mathrm{s^2\,m}}\frac{G}{c^4} \approx 8.2606 \times 10^{-39}\,\mathrm{km^{-2}}$$

$$[\rho]_{\mathrm{GU}} = [\rho]_{\mathrm{SI}} \cdot \frac{G}{c^2} = 1\,\frac{\mathrm{kg}}{\mathrm{m^3}}\frac{G}{c^2} \approx 7.424 \times 10^{-22}\,\mathrm{km^{-2}}$$

$$[M_\odot]_{\mathrm{GU}} = [M_\odot]_{\mathrm{SI}} \cdot \frac{G}{c^2} \approx 1.989 \times 10^{30}\,\mathrm{kg}\,\frac{G}{c^2} \approx 1.476\,\mathrm{km}.$$

Hence by defining the pressure P, energy density ϵ and mass M in units of kilometres

$$\overline{P} \equiv \frac{P\,G}{c^4}, \qquad\qquad \overline{\epsilon} \equiv \frac{\epsilon\,G}{c^2}, \qquad\qquad \overline{M} \equiv \frac{M\,G}{c^2}, \qquad (2.31)$$

we can rewrite the TOV equations (2.29) and (2.30) in geometrized units and obtain[2]

$$\frac{dy}{d\overline{P}} = \frac{-2\,y\,(\sqrt{y} - 2\overline{M})}{(\overline{\epsilon} + \overline{P})\,(\overline{M} + 4\pi\,y^{3/2}\,\overline{P})} \qquad (2.32)$$

$$\frac{d\overline{M}}{d\overline{P}} = \frac{-4\pi\,\overline{\epsilon}\,y^{3/2}\,(\sqrt{y} - 2\overline{M})}{(\overline{\epsilon} + \overline{P})\,(\overline{M} + 4\pi\,y^{3/2}\,\overline{P})}. \qquad (2.33)$$

---

[2] For clarity we use the following abbreviations: $y = y(\overline{P})$, $M = M(\overline{P})$, $\epsilon = \epsilon(\overline{P})$.

This system of ordinary differential equations can be solved by integrating over $\overline{P}$ with the two required initial values

$$y(\overline{P} = \overline{P}_c) = 0 \qquad \text{and} \qquad M(\overline{P} = \overline{P}_c) = 0\,, \qquad \text{with} \qquad \overline{P}(y = 0) := \overline{P}_c \qquad (2.34)$$

and the equation of state $\overline{\epsilon} = \overline{\epsilon}(\overline{P})$ as a further input. According to that, the radius and mass of the neutron star can be easily extracted by using the following equations:

$$R_{NS} = \sqrt{y(\overline{P} = 0)}, \qquad\qquad M_{NS} = M(\overline{P} = 0)\,. \qquad (2.35)$$

For a preferably good numerical integration, a small explicit step size and caution at the surface are necessary. Since the TOV equations have a singularity in $y = 0$, we use a leading order series expansion ($M(y) = 4\pi/3\epsilon y^{3/2}$ with $y \approx 0$) as the first step. It can be said that the solution of the TOV equations only depends on the central pressure P_c and the equation of state $\epsilon(P)$. Modifying P_c will lead to different tuples (R_{NS}, M_{NS}) which can be visualized in the M,R - plane. The resulting graph is called mass-radius (MR) curve in which every point represents a single neutron star with a different central pressure. These mass-radius curves are unique for every single equation of state.

In this thesis the described method for solving the TOV equations is realized in the programming language *Python*. To solve the system of ordinary differential equations a built-in feature using *lsoda* is used.
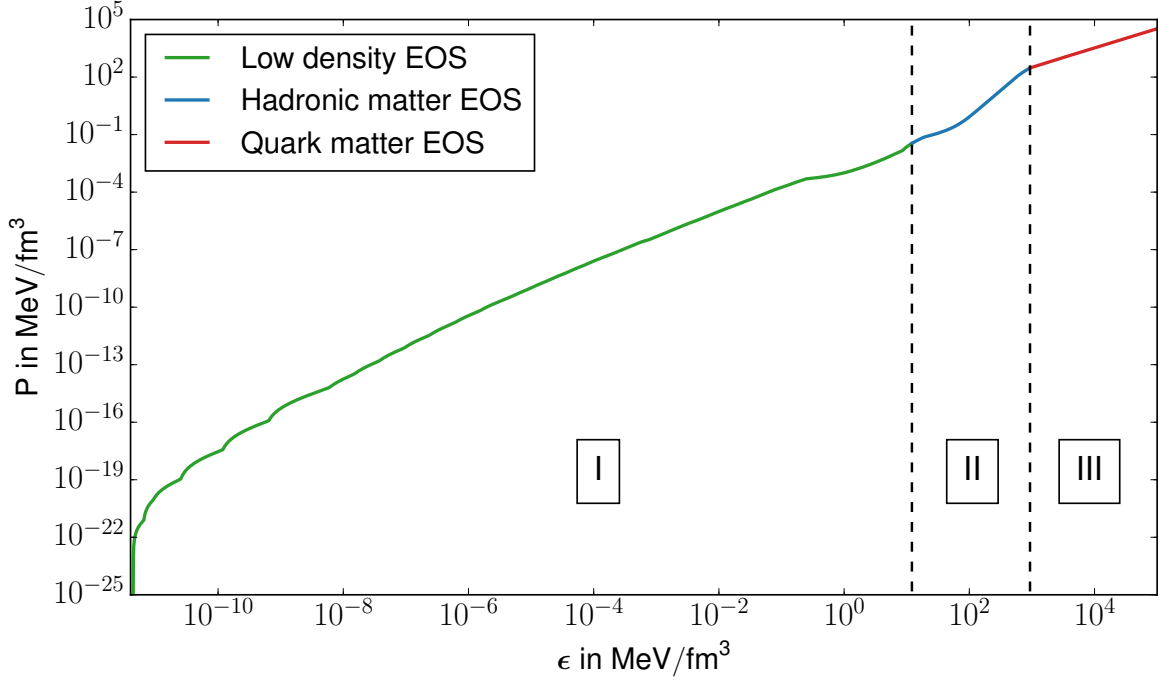
2.4 Equation of state

An equation of state puts the various thermodynamic quantities in relation. Within the scope of this thesis, we are mainly interested in the relation between the pressure P and the energy density ϵ, since they are needed as input parameters of the TOV equations. The EoS depends on the interactions between the particles and the temperature. Since it is not possible to reproduce cold matter at high densities well beyond ρ_0 in laboratory (particle accelerators), we have no way to experimentally examine matter at these densities. The uncertainties of the EoS increase enormously in this region [25]. Therefore there exist a lot of different theories trying to describe matter at these densities. Some of them will be discussed in Section 2.4.2. One way to distinguish equations of state is comparing the compressibility. We differ between soft, moderate and stiff EoSs. For a given energy density, stiff EoSs reach higher pressures than softer ones. Moreover a stiff EoS provides larger masses M_{NS}. In this work we will divide the EoS in three parts (see Figure 2.3) with respect to the baryon density n, where n_0 describes the saturation density:

  I. Low-density EoS up to $0.05\,n_0$

 II. Hadronic EoS from $0.05\,n_0$ to the phase transition to quark-matter

III. Quark EoS for all particle densities above the phase transition

In this thesis we assume, that the phase transition from hadronic to quark matter occurs at densities between $(1-7)\,n_0$.

Figure 2.3: Subdivision of the equation of state in a low-density EoS (I), a hadronic EoS (II) and a quark EoS (III). In this figure we us for the low-density EoS the BPS EoS, for the hadronic EoS the BHF(N,l) EoS and for the quark EoS a CSS EoS (see Section 2.4.2). The phase transition to the deconfined phase occurs at n = 4.82 n$_0$.

2.4.1 Necessary conditions for the equation of state

With reference to the paper of Rhoades and Ruffini [26], we will summarize some necessary conditions for the EoS:

- Perturbations from the equilibrium must not destabilize the matter (principle of Le Chatelier). This generally means that the EoS is an increasing function with respect to the energy density

$$\frac{\mathrm{d}P}{\mathrm{d}\epsilon} \geq 0 \,. \tag{2.36}$$

The equality of equation (2.36) is only allowed in case of a first-order phase transition.

- The EoS must satisfy the principle of causality. This means that the velocity of sound v_s is below the speed of light c

$$\frac{v_s}{c} = \sqrt{\frac{\mathrm{d}P}{\mathrm{d}\epsilon}} \leq 1 \,. \tag{2.37}$$

- The EoS must fulfill the thermodynamical constraints, particularly the relation of Gibbs-Duhem (for T = 0): $N\mathrm{d}\mu = V\mathrm{d}P$ with the Volume V, the Number of particles N and the chemical potential μ. Furthermore the pressure as a function of μ must be continuous everywhere [5].

With these assumptions we can find $M_{max} = 3.14\,M_\odot$ as maximal mass of a causal neutron star [12]. If we neglect the principle of causality, the EoS could be much stiffer and the maximal mass would be around $5\,M_\odot$ [27].

2.4.2 Used equations of state

In this thesis we will use the following EoSs, which in combination fulfill the conditions of Section 2.4.1. We will only give a short overview of the key properties for the used EoSs since their details go far beyond the level of this work. For further information the used sources are recommended.

Low density EoS

For subnuclear densities in the crust, we choose the EoS of Baym-Pethick-Sutherland [28]. This EoS describes charge-neutral hadronic matter in its ground state. Since iron has the highest binding energy per nucleon, it is the endpoint of nuclear burning and the ground state of matter for low pressure [12]. Therefore at zero pressure the energy density is $\epsilon(P = 0)_{BPS} = \epsilon_{Fe} = 4.41 \times 10^{-12}\,\mathrm{MeV\,fm^{-3}}$. In contrast to Section 2.1.1, the surface of the neutron star described by the BPS EoS consists of iron without any atmosphere. The BPS equation of state is tabulated in [12].

Hadron matter EoS
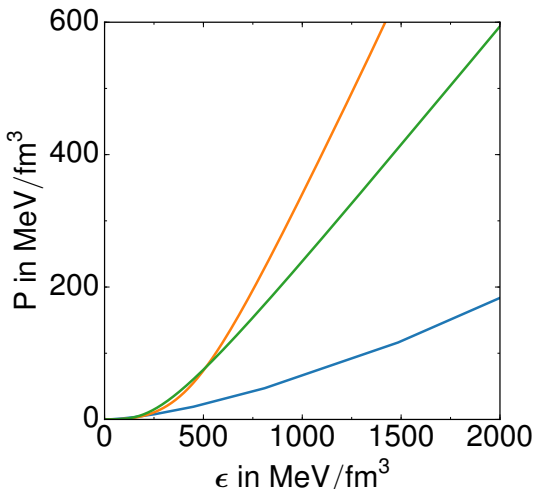
Figure 2.4: The used EoSs BHF(N,l) (orange line) and χ SU(3) (green line) in comparison to the ideal neutron gas (blue line).

In this work we will use two different hadronic EoSs. The first one is the **BHF(N,l)** equation of state, which was derived from the non-relativistic Brueckner-Bethe-Goldstone many-body theory using the Brueckner-Hartree-Fock approximation [29]. It is a microscopic EoS which includes nucleons and non-interacting leptons. The second EoS bases on a non-linear chiral SU(3) symmetry and contains hyperons [30, 31, 32]. Analogously to [33] we denote this EoS χ **SU(3)**. Both EoSs are interpolated to match continuously to the BPS EoS at low densities. In Figure 2.4 the two EoSs are compared to the ideal neutron gas[3]. The BHF(N,l) EoS is stiffer, the χ SU(3) is softer. The free neutron gas is an excessively soft equation of state, as the repulsive forces at small distances between the particles are not considered.

---

[3]   The derivation of this EoS can be inferred by [12, 34]. For this EoS we do not use the BPS EoS.

For the quark matter we use **constant speed of sound (CSS)** EoSs. They base on the following assumption

$$c_{QM}^2 := \left(\frac{v_s}{c}\right)^2 = \frac{dP}{d\epsilon} = \text{const.}, \quad \text{for all } \epsilon. \tag{2.38}$$

As mentioned in Section 2.4.1, c_{QM}^2 is bounded through 0 and 1. In this thesis we will use two different sound velocities for the quark matter EoS. The first value is the causal limit $c_{QM}^2 = 1$. For the second value we will use $c_{QM}^2 = 1/3$. At high densities a principle characteristic of QCD appears, the asymptotic freedom. The coupling of the quarks becomes less with increasing densities. Quarks and gluons behave like a relativistic gas with the EoS $P = \epsilon/3$ [25].

To prove the justification of the usage of CSS EoS, we will now analyze the sound velocity of a few deconfined quark matter EoSs using the (2+1)-flavor Nambu-Jona-Lasinio (NJL) model.

(a) The quark matter EoSs.

(b) The sound velocities c_{QM}^2 of the quark EoSs.
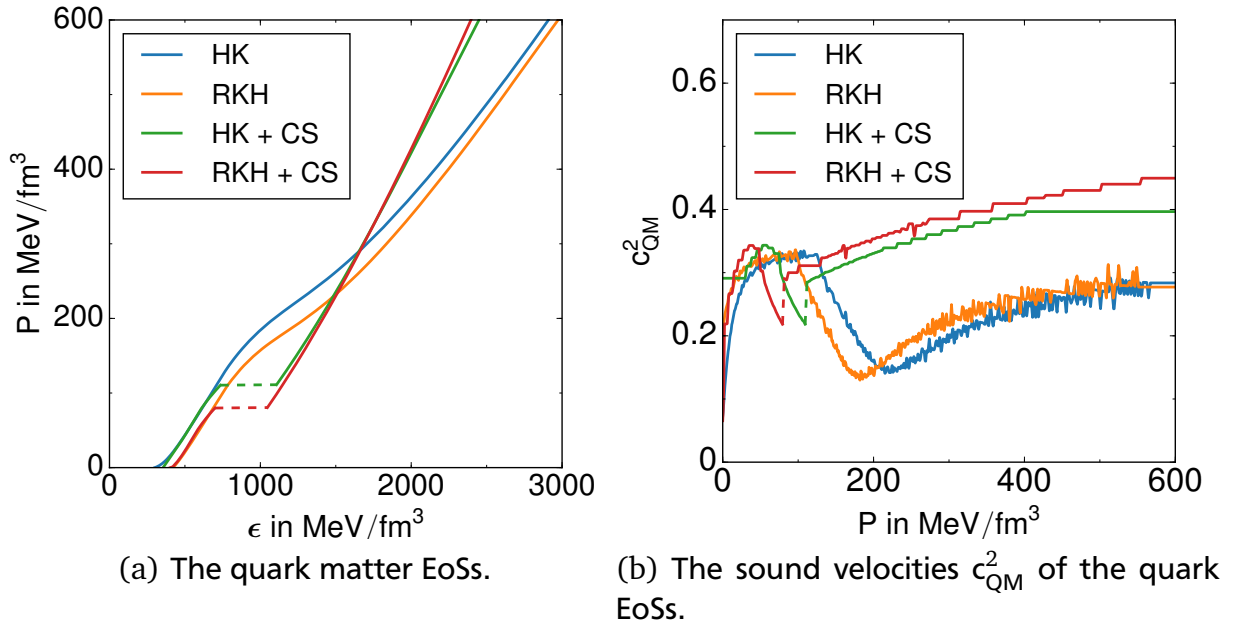
Figure 2.5: The quark matter EoSs HK, HK + CS, RHK, RHK + CS in (a) and their sound velocity c_{QM}^2 in (b).

The Nambu-Jona-Lasinio (NJL) model refers to the work of Nambu and Jona-Lasinio [35, 36]. According to [33], the NJL model describes cold, strongly interacting quark matter containing up, down and strange quarks. The EoSs introduced in [33] are shown in Figure 2.5(a), based on two different sets of NJL parameter (RKH) and (HK) and can be extended to describe color superconductivity (CS) [33]. For low densities the two-flavor color superconductivity (2SC) phase dominates and for high densities the color-flavor locked (CFL) condensate. A phase transition of first-order occurs between the two phases.

The sound velocities of the four NJL EoSs are shown in Figure 2.5(b). The vibrations of the curves result from the interpolation of the quark matter EoS of finite points. Due to the phase transition from 2SC to CFL, the EoSs and sound velocities with CS show discontinuities. For pressures up to $300\,\mathrm{MeV/fm^3}$ ($n \approx 5\,n_0$) the sound velocities vary about 0.15. For higher densities, c_{QM}^2 is nearly independent of the pressure and converges to $c_{QM}^2 \approx 0.3$ (without CS) respectively $c_{QM}^2 \approx 0.4$ (with CS). For this reason the CSS EoS is at least justifiable for high densities $n \gtrsim 5\,n_0$.

## 2.5 Mass-radius curves

A mass-radius curve is defined as the tuple $(M_{NS}(P_c), R_{NS}(P_c))$ as a function of the central pressure P_c. The mass and radius of a neutron star is calculated as explained in Section 2.3. In the following we will establish whether a neutron star with the parametres $(M_{NS}(P_c), R_{NS}(P_c), P_c)$ is stable or not. Afterwards we will show some mass-radius curves and analyze their validity.

2.5.1 Conditions for stable neutron stars

There are necessary and sufficient conditions for stability [12]:

A neutron star is held together by the equilibrium of the gravitational force and force caused by the pressure depending on the EoS. Referring to Figure 2.6 we suppose an equilibrium solution S of the TOV equations. Due to a perturbation the central energy density ϵ_c is increased. The star is therefore compressed C and the equilibrium star with the increased energy density would belong to C*. Since the Star C has an deficit in mass against the equilibrium solution S, the gravity force is less than the pressure force. Therefore the gravitational force will act to return it to S. Similarly, we can argue that a perturbed star with a lower central density will act to return to S by the force acting on the matter. By a similar argument of the star U in the decreasing curve of M, we can say that, if either the star is compressed or decompressed, the force acting on the matter will drive it further from U. In conclusion we can say that a neutron star is stable as long as the mass is an increasing function of the central energy density ϵ_c. Hence the **necessary condition for stability** is
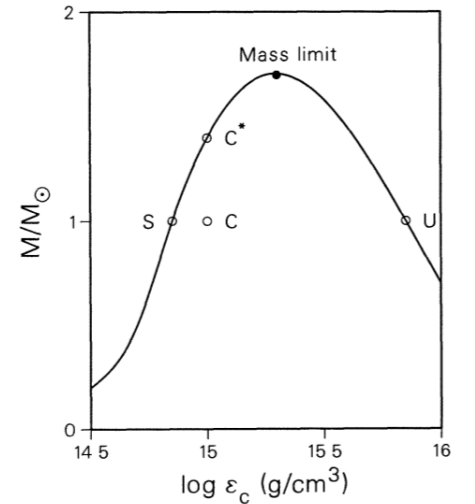
Figure 2.6: Schematic of a TOV solution with increasing and decreasing mass as a function of ϵ_c [12].

$$\frac{dM}{d\epsilon_c} \geq 0 \quad \Leftrightarrow \quad \frac{dM}{dP_c} \geq 0 \quad \Leftrightarrow \quad \frac{dM}{dn_c} \geq 0\,. \tag{2.39}$$

Beside the hydrostatic stability described by Equation (2.39), the star must be dynamically stable. A **sufficient condition for stabilty** is that the neutron star is stable against normal radial modes of vibration (acoustical modes) [1]. We will concretize this in Section 2.5.2 by outlining consequences on the mass-radius curves.

In general we can say that for neutron stars with low masses, the radii are larger than for stars with large masses. In a star with a low mass the central pressure is comparatively low and the gravitational force reaches the equilibrium configuration at large radii. Analogously for massive stars the central pressure is high and the gravitational force will shift the state of equilibrium to small radii. We will now discuss the mass-radius curves of three different EoSs pictured in Figure 2.7. The corresponding mass central pressure (MP$_c$) curve is shown in Figure 2.8. In both figures the masses of the neutron stars PSR B1913+16 (M = 1.44 M$_\odot$ [37]) (also called Hulse-Taylor pulsar) and PSR J1614-2230 (M = (1.97 ± 0.04) M$_\odot$ [3]) are shown.
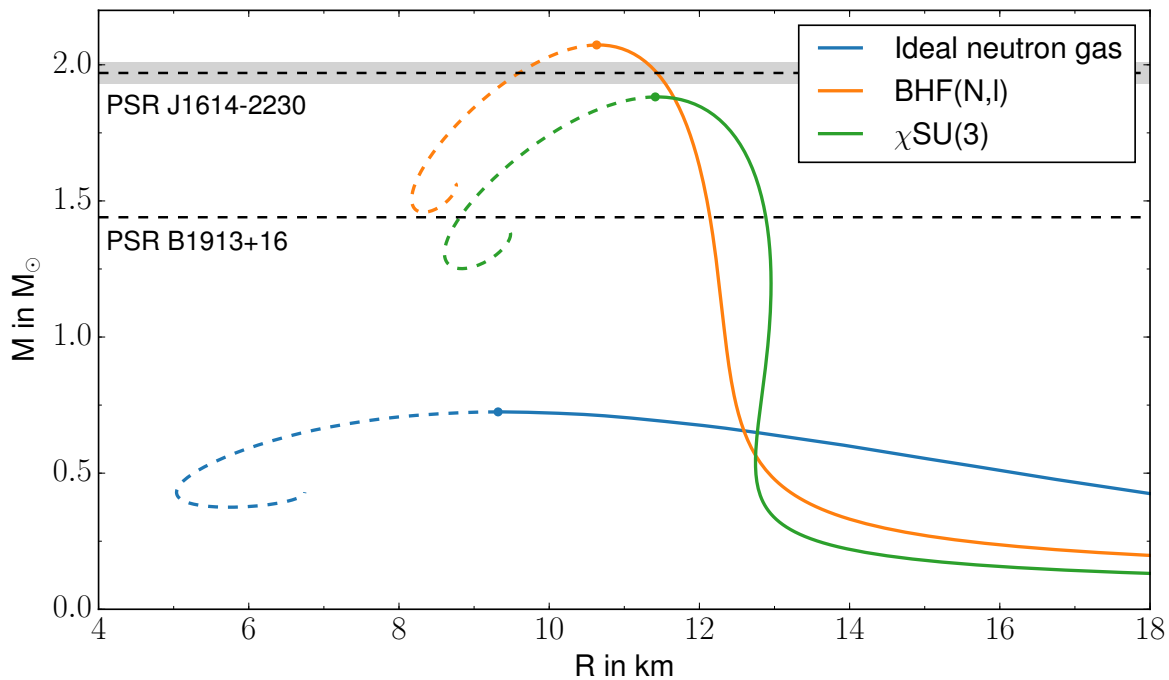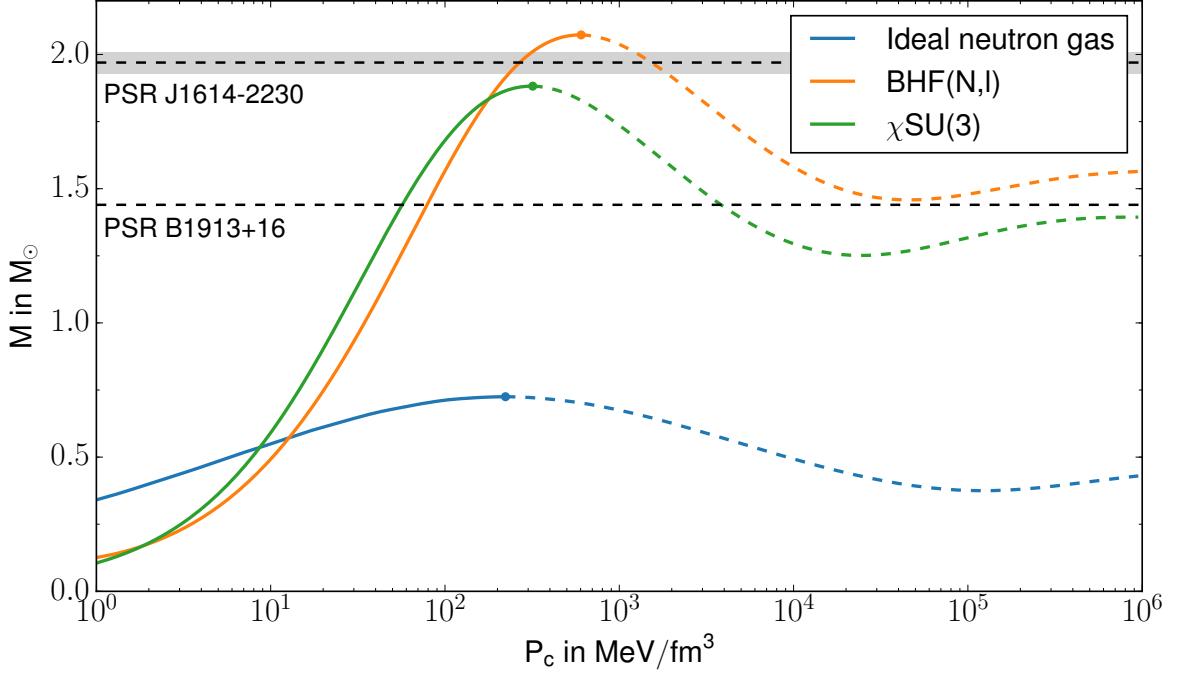

Figure 2.7: Mass-radius curves of the ideal neutron gas, the BHF(N,l) EoS and the χ SU(3) EoS in comparison to the mass of the neutron stars PSR B1913+16 and PSR J1614-2230 with their uncertainties. The stable equilibrium configurations are characterized by a continuous line, the unstable by a dashed line. The point of the maximal stable mass is marked as a dot. Following the curves from large radii to low radii, the central pressure increase.

The blue graph indicates the MR curve of the **free neutron gas**. The maximal stable mass of this EoS is M = 0.72 M$_\odot$ at a radius of R = 9.32 km. The ideal neutron gas does neither accommodate the Hulse-Taylor pulsar nor fit to the average neutron star mass $\overline{M}_{NS} = (1.350 \pm 0.004)$ M$_\odot$ deduced from the observation of radio pulsar systems by Thorsett and Chakrabarty [38]. Therefore the free neutron gas fails for being a realistic EoS of a neutron star.

We will now come to more realistic EoS which can reproduce the Hulse-Taylor pulsar or even more massive neutron stars like the PSR J1614-2230. The BHF(N,l) equation of state is presented by the orange and the χ SU(3) EoS by the green graph in Figure 2.7. The main properties of these equations of state and of the corresponding neutron stars are summarized in Table 2.1. The two EoSs (Figure 2.4) themselves already indicate that the BHF EoS is the stiffer one. This

fact also occurs in the MR curves since the BHF EoS can describe higher masses.

Figure 2.8: Mass central pressure curves of the ideal neutron gas, the BHF(N,l) EoS and the $\chi\,SU(3)$ EoS in comparison to the mass of the neutron stars PSR B1913+16 and PSR J1614-2230 with their uncertainties. The stable equilibrium configurations are characterized by a continuous line, the unstable by a dashed line. The point of the maximal stable mass is marked as a dot.

Property	BHF(N,l)	$\chi\,SU(3)$
Saturation baryon density n_0	$0.176\,\mathrm{fm}^{-3}$	$0.15\,\mathrm{fm}^{-3}$
Binding energy per baryon E/A	$-16.01\,\mathrm{MeV}$	$-16.00\,\mathrm{MeV}$
Incompressibility K	$281\,\mathrm{MeV}$	$276\,\mathrm{MeV}$
Maximum mass M_{max} of star	$2.07\,\mathrm{M_\odot}$	$1.88\,\mathrm{M_\odot}$
Radius R_{max} of the heaviest star	$10.63\,\mathrm{km}$	$11.41\,\mathrm{km}$
Central baryon density n_c of the heaviest star	$6.57\,n_0$	$5.96\,n_0$
Central pressure p_c of the heaviest star	$604.42\,\mathrm{MeV\,fm}^{-3}$	$318.71\,\mathrm{MeV\,fm}^{-3}$
Central energy density ϵ_c of the heaviest star	$1427.05\,\mathrm{MeV\,fm}^{-3}$	$1228.45\,\mathrm{MeV\,fm}^{-3}$
Radius r_{HTp} of the Hulse-Taylor pulsar	$12.14\,\mathrm{km}$	$12.88\,\mathrm{km}$

Table 2.1: The principle properties of the BHF(N,l) and $\chi\,SU(3)$ EoS [29, 30, 31, 32] and the corresponding NS. $\chi\,SU(3)$ is softer, BHF(N,l) is stiffer.

By analyzing the MP_c curves of Figure 2.8, we determine that for increasing P_c at very high central pressures, the masses increase as well. Although the necessary condition for a stable star configuration (Equation (2.39)) is fullfilled, neutron stars with these high central pressures are unstable. In this context we will now present the details of the sufficient condition of stable neutron stars according to [1]. In Figure 2.9 the stable and unstable mass-radius relations of compact stars are shown. At every critical point ($dM/dP_c = 0$, denoted by A, B, ..., I) a vibrational mode changes its stability. If at a critical point $dR/dP_c < 0$ holds, the lowest even mode will be changed. If in contrast $dR/dP_c > 0$ holds, the lowest odd mode will be changed [1]. A star can only be considered as stable against radial perturbations if all vibrational modes are stable. Therefore mass-radius relations with a curvature comparable to the curve B-C-H-I (see Figure 2.7) are unstable after reaching point C, although the necessary stability condition (2.39) is satisfied after point H. To obtain another stable sequence of compact stars at lower radii, the MR relation must show a behavior like the curve B-C-D-E. In the next chapter we will see that a phase transition to deconfined matter can lead to this curvature.
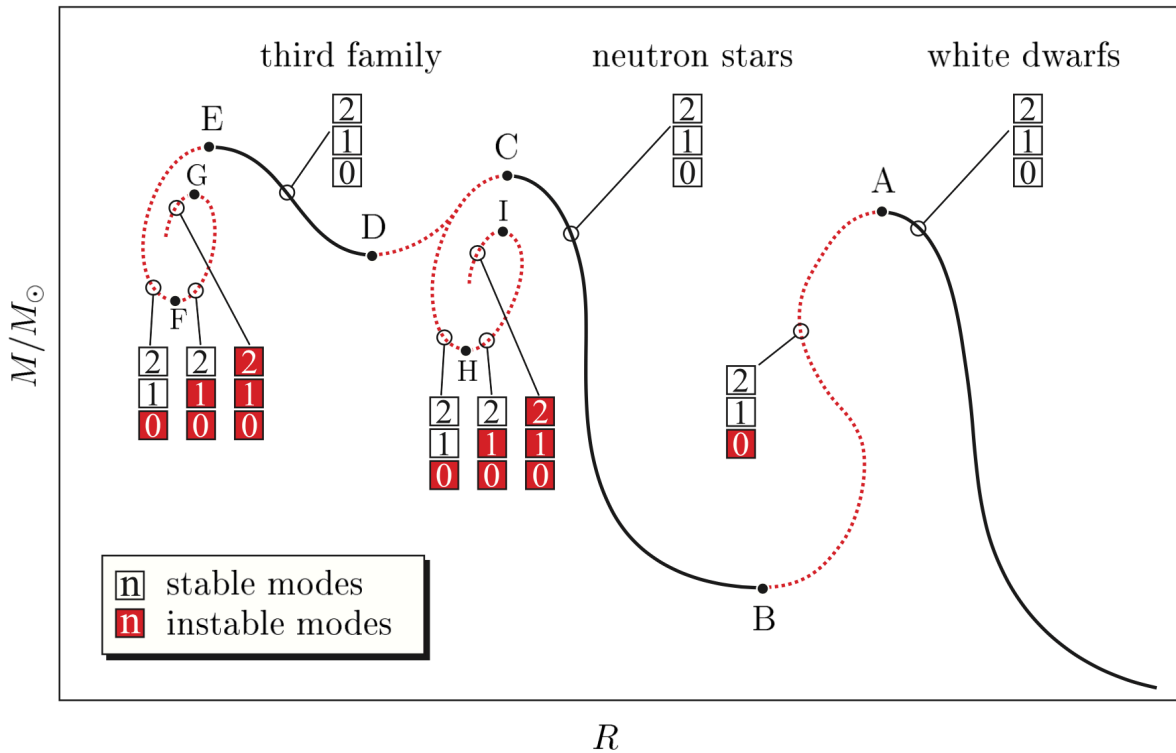
Figure 2.9: Schematic of possible mass-radius relations for compact stars taken from [1]. Stable star configurations are indicated by black solid lines, unstable TOV solutions by red dotted lines. The points A, B, ..., I refer to the critical turning points. The stability of the lowest three vibrational modes are specified for every part of the MR curve between two critical points. All higher vibrational modes are stable.

3 "Third family" stars induced by a first-order phase transition

In this chapter we analyze the mass-radius curves and the occurrence of "third family" stars, due to a phase transition of first-order from hadron matter to a deconfined quark matter. First of all we discuss this phase transition at constant pressure and parametrize it. For certain transition parameters the star destabilizes immediately after the phase transition. We derive a criterion which specifies the values of the parameters for this case. Varying the transition parameters of the phase transition leads in general to four different kinds of MR curves: A, B, C and D. The occurrence of regions A, B, C and D can be displayed in dependency on the transition parameters. We denote this the "phase" diagram. Two of the four MR cases contain "third family" stars. For these regions we investigate the observables of "third family" stars like mass or radius. Finally we analyze "neutron star twins" and carve out different characteristics.

3.1 The parameterization of the equation of state

As described in Section 2.4.2 we will use an equation of state, consisting of the BPS EoS for the crust, a hadronic EoS (BHF(N,l) or χ SU(3)) and the CSS EoS for the quark matter. Before we can parameterize the phase transition from hadron to quark matter, we have to analyze the first-order phase transition. Afterwards we will derive more details about the CSS EoS as a function of the parameterization.

3.1.1 first-order phase transition

In this thesis we assume a sharp interface between the two phases. The Maxwell construction is used, which means that the first-order phase transition occurs at a specific pressure. At this transition point the System is arranged to be in a chemical, thermal and mechanical equilibrium. According to Gibbs the chemical potentials, the temperatures and the pressures are equal at the transition point [12]

$$\mu_{HM} = \mu_{QM}, \quad T_{HM} = T_{QM}, \quad P_{HM} = P_{QM}, \tag{3.1}$$

where the index HM and QM denote the hadron and quark phases. Due to Equation (3.1) the phase change is called constant pressure phase transition. In general the energy and baryon densities ϵ and n do not have to be continuous at the transition pressure [12].
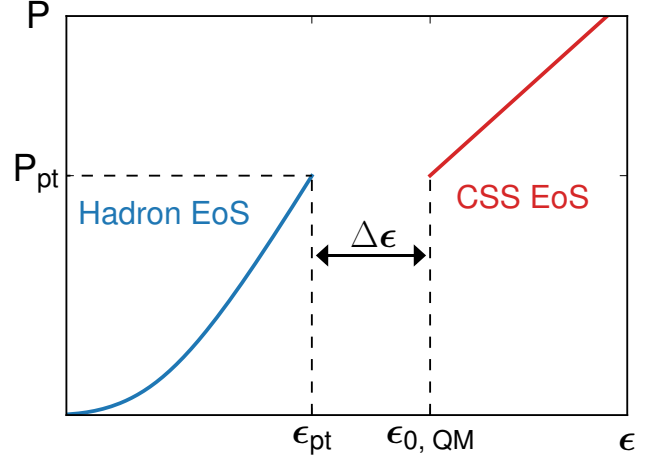
3.1.2 The CSS parametrization

With reference to Figure 3.1, we parametrize the hybrid equation of state ϵ_{CSS} containing a first-order phase transition as follows:

The constant pressure phase transition occurs at the pressure P_{pt}. For $P \leq P_{pt}$, ϵ_{CSS} conforms with the hadron EoS $\epsilon_{HM}(P)$. For $P > P_{pt}$, the hybrid EoS ϵ_{CSS} is equal to a quark matter CSS EoS $\epsilon_{QM}(P)$ with $dP/d\epsilon_{QM} = c_{QM}^2$. Between the two energy densities $\epsilon_{pt} := \epsilon_{HM}(P_{pt})$ and $\epsilon_{0,QM} := \epsilon_{QM}(P_{pt})$, there is an energy density discontinuity $\Delta\epsilon = \epsilon_{0,QM} - \epsilon_{pt}$. To achieve these properties, we define the equation of state as follows:

Figure 3.1: Hybrid EoS containing a first-order phase transition from hadron matter (blue) to quark matter (red) defined by the transition pressure P_{pt} and the energy discontinuity $\Delta\epsilon$.

$$\epsilon_{CSS}(P) = \begin{cases} \epsilon_{HM}(P) & , P < P_{pt} \\ \dfrac{P - P_{pt}}{c_{QM}^2} + \epsilon_{pt} + \Delta\epsilon & , P > P_{pt} \end{cases} \tag{3.2}$$

c_{QM}^2 denotes the sound velocity defined in Equation (2.38). If the hadron matter EoS and the sound velocity c_{QM}^2 for the quark matter EoS are known, the equation of state is determined by the two parameters P_{pt} and $\Delta\epsilon$.

3.1.3 Chemical potential and particle density of the CSS EoS

For the following calculations we need the dependency on the chemical potential μ and particle density n on the pressure P of the CSS parametrization. For the derivation we use some fundamental thermodynamical definitions and relations assuming cold stars (T = 0) [34]:

$$\text{Gibbs-Duhem-relation:} \qquad Nd\mu = VdP \tag{3.3}$$

$$\text{Particle density:} \qquad n = \frac{N}{V} = \frac{dP}{d\mu} \tag{3.4}$$

$$\text{Pressure:} \qquad P = -\left.\frac{\partial E}{\partial V}\right|_n \tag{3.5}$$

$$\text{Chemical potential:} \qquad \mu = \left.\frac{\partial E}{\partial N}\right|_V = \left.\frac{\partial \epsilon}{\partial n}\right|_V \tag{3.6}$$

We can rewrite the pressure $P = P(\epsilon)$

$$P = -\frac{\partial(\epsilon/n)}{\partial(1/n)} = n^2 \frac{\partial}{\partial n}\left(\frac{\epsilon}{n}\right) = n\mu - \epsilon \qquad \Longleftrightarrow \qquad \frac{dP}{d\mu} = \frac{P + \epsilon(P)}{\mu}. \tag{3.7}$$

From the differential equation (3.7), we obtain $P(\mu)$ by using $\epsilon(P) = (P - P_{pt})/c_{QM}^2 + \epsilon_{pt} + \Delta\epsilon$ and the abbreviations $D = -P_{pt}/c_{QM}^2 + \epsilon_{pt} + \Delta\epsilon$ and $F = (1 + c_{QM}^2)/c_{QM}^2$

$$P(\mu) = -\frac{D}{F} + \mu^F C. \tag{3.8}$$

The constant of integration C is fixed by the condition $P(\mu_{pt}) = P_{pt}$. Since $\mu_{pt} = (P_{pt} + \epsilon_{pt})/n_{pt}$ and Equation (3.1) holds for a first-order phase transition, we obtain

$$P(\mu) = -\frac{D}{F} + \left(P_{pt} + \frac{D}{F}\right)\left(\frac{\mu}{\mu_{pt}}\right)^F \qquad \Leftrightarrow \qquad \mu_{CSS}(P) = \mu_{pt}\left(\frac{PF + D}{P_{pt}F + D}\right)^{1/F}. \qquad (3.9)$$

Now we can compute the particle density $n_{CSS}(P)$ from Equation (3.4)

$$n_{CSS}(P) = \left(\frac{d\mu(P)}{dP}\right)^{-1} = \frac{P_{pt}F + D}{\mu_{pt}}\left(\frac{PF + D}{P_{pt}F + D}\right)^{1/(F c_{QM}^2)}. \qquad (3.10)$$

As we can see in Figure 3.2, the pressure and the chemical potential is continuous at the phase transition as expected from Equation (3.1). The energy and particle density are not continuous.
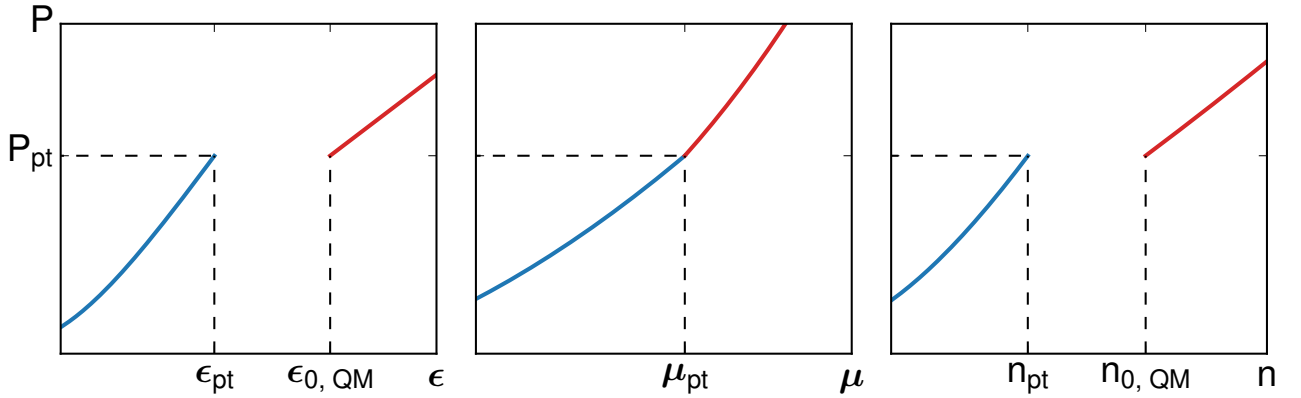
Figure 3.2: Schematic of the pressure P as a function of the energy density ϵ, the chemical potential μ and the particle density n in case of a first-order phase transition from a hadronic phase (blue) to the CSS quark phase (red).

3.2 Generic conditions for stable hybrid stars

Based on the work of Seidov in 1970 [39], we derive a criterion for stable hybrid stars with a vanishingly small quark core induced by a first-order phase change. A more detailed derivation is shown in [40, 41]. In the following we use the Tolman-Oppenheimer-Volkoff equations with respect to r in geometrized units

$$\frac{dP}{dr} = -\frac{(P+\epsilon)(M+4\pi r^3 P)}{r(r-2M)}, \qquad \frac{dM}{dr} = 4\pi r^2 \epsilon. \qquad (3.11)$$

We assume a phase transition as defined in Equation (3.2) and denote all quantities of the star as before. For $P_c > P_{pt}$ there exists a core with radius r_N consisting of a quark matter phase. Assuming $P_c - P_{pt} = \delta \ll P_{pt}$ and $r_N \ll R_{NS}$, we define $P_+(r)$ as the solution for this case. In contrast, $P_-(r)$ denotes the boundary solution for a homogeneous star with $P_c = P_{pt}$. In a small neighborhood of the centre of a homogeneous star, we can approximate the solution $P_-(r)$.

Using $P(r) = P_{pt}$, $\epsilon(P_{pt}) = \epsilon_{pt}$ and $M = 4\pi/3 r^3 \epsilon_{pt}$ we rewrite (3.11) and expand it to the leading order

$$\frac{dP_-}{dr} = -\frac{4\pi}{3}\frac{(P_{pt} + \epsilon_{pt})(3P_{pt} + \epsilon_{pt})}{(\frac{1}{r} - \frac{8\pi}{3}r\epsilon_{pt})} \tag{3.12}$$

$$\approx \left.\frac{dP_-}{dr}\right|_{r=0} + \left.\frac{d^2 P_-}{dr^2}\right|_{r=0} \cdot r = -\frac{4\pi}{3}r(P_{pt} + \epsilon_{pt})(3P_{pt} + \epsilon_{pt}). \tag{3.13}$$

Integrating Equation (3.13) from $r' = 0$ to r we obtain

$$P_-(r) = P_{pt} - \delta_-(r), \qquad \text{with} \qquad \delta_-(r) = \frac{2\pi}{3}(P_{pt} + \epsilon_{pt})(3P_{pt} + \epsilon_{pt})r^2. \tag{3.14}$$

Analogously for the derivative of $P_+(r)$ at radius $r = r_N$ with $P_+(r_N) = P_{pt}$, $\epsilon(P_{pt}) = \epsilon_{pt}$ and $M = 4\pi/3 r^3 \epsilon_{0,\,QM}$ yields

$$\left.\frac{dP_+}{dr}\right|_{r=r_N} = -\frac{4\pi}{3}r_N(P_{pt} + \epsilon_{pt})(3P_{pt} + \epsilon_{0,\,QM}). \tag{3.15}$$

Doing the same expansion and integration for $P_+(r)$ on the quark matter side, we obtain

$$P_+(r) = P_c - \delta_+(r), \qquad \text{with} \qquad \delta_+(r) = \frac{2\pi}{3}(P_{pt} + \epsilon_{0,\,QM})(3P_{pt} + \epsilon_{0,\,QM})r^2. \tag{3.16}$$

Using $P_+(r_N) = P_{pt}$ we finally get the dependence of δ on r_N

$$\delta = P_c - P_{pt} = \frac{2\pi}{3}(P_{pt} + \epsilon_{0,\,QM})(3P_{pt} + \epsilon_{0,\,QM})r_N^2. \tag{3.17}$$

To express the solution $P_+(r)$ by a known solution $P_-(r)$, we apply perturbation theory with the perturbation function $\Pi(r)$

$$P_+(r) = P_-(r) + \Pi(r). \tag{3.18}$$

Substituting $P_+(r) = P_-(r) + \Pi(r)$ in Equation (3.11), assuming small r and neglecting terms proportional to Π^2 and $\Pi \, d\Pi/dr$, it can be shown [42] that the perturbation function has the form: $\Pi(r) = G + H/r$.
Therefore we can estimate the approximation of $P_+(r)$ and its derivative at the radius r_N

$$\left.\begin{array}{l} P_{pt} = P_{pt} - \delta_-(r_N) + G + \dfrac{H}{r_N} \\[2mm] \left.\dfrac{dP_+}{dr}\right|_{r=r_N} = -\left.\dfrac{d\delta_-}{dr}\right|_{r=r_N} - \dfrac{H}{r_N^2} \end{array}\right\} \quad \Rightarrow \quad G = \delta_-(r_N) + r_N\left(\left.\frac{dP_+}{dr}\right|_{r=r_N} + \left.\frac{d\delta_-}{dr}\right|_{r=r_N}\right). \tag{3.19}$$

Using Equations (3.14), (3.15) and (3.17) we obtain

$$G = \frac{(2 + \frac{P_{pt}}{\epsilon_{pt}})(3\frac{P_{pt}}{\epsilon_{pt}} + 1 - 2\frac{\Delta\epsilon}{\epsilon_{pt}})}{(\frac{\Delta\epsilon}{\epsilon_{pt}} - 1 + \frac{P_{pt}}{\epsilon_{pt}})(\frac{\Delta\epsilon}{\epsilon_{pt}} - 1 + 3\frac{P_{pt}}{\epsilon_{pt}})}\delta. \tag{3.20}$$

For radii $r \gg r_N$, the perturbation function approaches $\Pi(r) \approx G$. Consequently $P_+(r)$ conforms with the solution $P_-(r)$ of a homogeneous star with no phase transition and a central pressure value $P_c = P_{pt} + F$. Hence we obtain the following relation for the left and right derivatives of the neutron star mass with respect to the central pressure at the point $P_c = P_{pt}$

$$\frac{dM_{NS,+}}{dP_c} = \frac{(2 + \frac{P_{pt}}{\epsilon_{pt}})(3\frac{P_{pt}}{\epsilon_{pt}} + 1 - 2\frac{\Delta\epsilon}{\epsilon_{pt}})}{(\frac{\Delta\epsilon}{\epsilon_{pt}} - 1 + \frac{P_{pt}}{\epsilon_{pt}})(\frac{\Delta\epsilon}{\epsilon_{pt}} - 1 + 3\frac{P_{pt}}{\epsilon_{pt}})} \frac{dM_{NS,-}}{dP_c}. \tag{3.21}$$

If we assume a stable neutron star consisting of pure hadronic matter $(dM_{NS,-}/dP_c > 0)$, then its counterpart with a vanishingly small quark matter core is only stable $(dM_{NS,+}/dP_c > 0)$ if $\Delta\epsilon < \Delta\epsilon_{crit}$ with

$$\frac{\Delta\epsilon_{crit}}{\epsilon_{pt}} = \frac{1}{2} + \frac{3}{2}\frac{P_{pt}}{\epsilon_{pt}}. \tag{3.22}$$

Therefore, if the energy density discontinuity of the phase transition is larger than this critical value, the neutron star will be destabilized immediately by a small quark matter core. Since we derived equation (3.22) by using many approximations, it is an essential task for the following section to prove this criterion by calculating mass-radius curves using the TOV equations.

3.3 The "phase" diagram

We will now discuss and characterize the four different types of mass-radius curves for hybrid stars as defined in [43]. The occurrence of the different types will be presented in a "phase" diagram depending on the phase transition parameters introduced in Section 3.1.2. Hence we can extract necessary conditions for the occurrence of "third family" stars. After that we analyze the dependency on this "phase" diagram on different hadron EoSs and quark matter sound velocities c_{QM}^2.

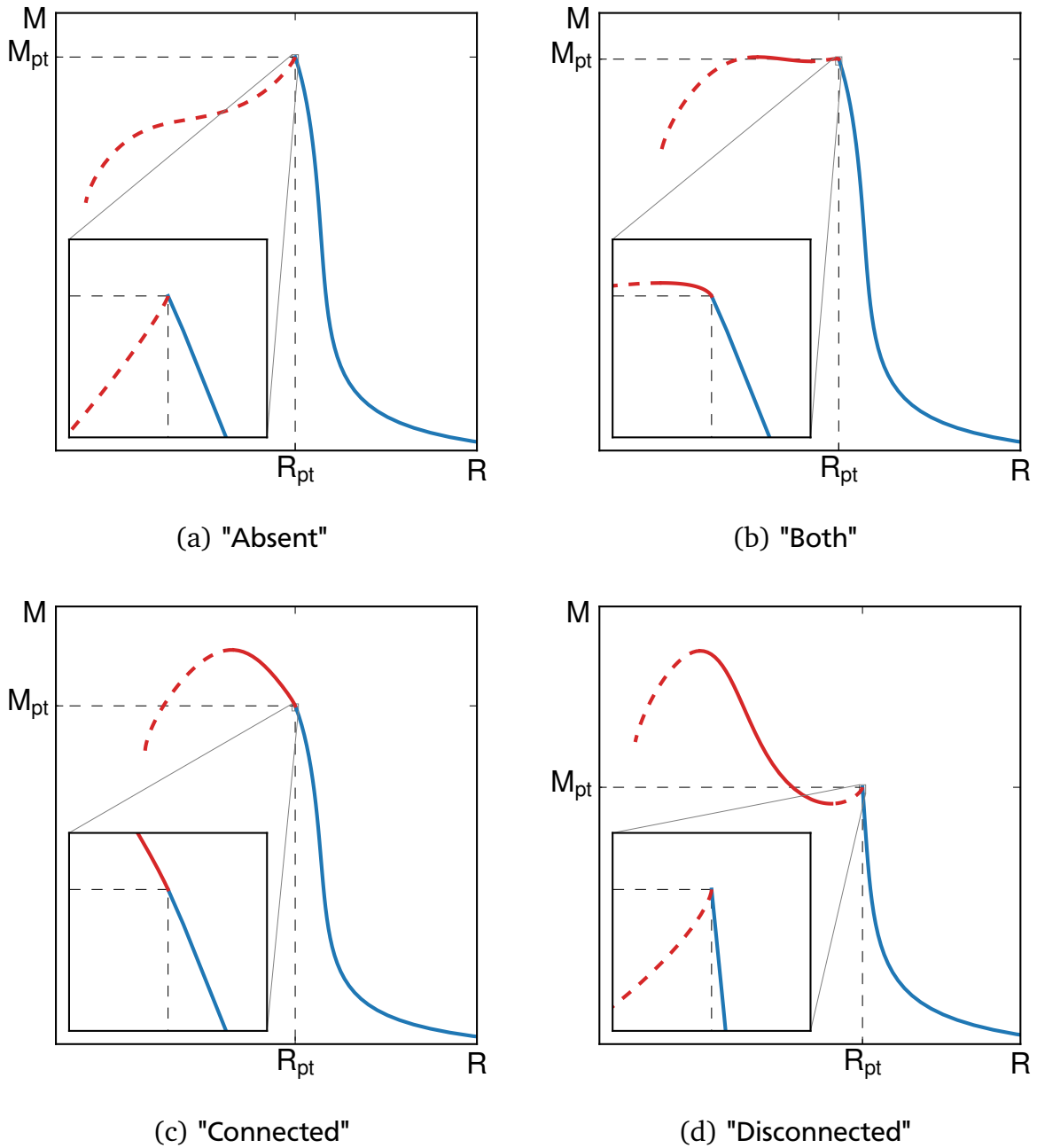### 3.3.1 Different possible mass-radius relations of hybrid stars

Varying the values of the transition pressure P_{pt} and the energy discontinuity $\Delta\epsilon$ over a broad range, we can classify four different types of mass-radius curves. Analogously to [43] we denote the different types A, B, C and D. These types are presented in Figure 3.3 and will be discussed in the following.

The first possibility is that there is no stable hybrid star at all. The occurrence of a vanishingly small quark matter core destabilizes the whole star. Even if the quark core grows, the hybrid star stays destabilized. We denote this case "**Absent**" **(A)** and display it in Figure 3.3(a).

Analogously to the previous case, stars of type **(D)** "**Disconnected**" destabilize by the appearance of quark matter in the interior. But in contrast to A, there exists a stable equilibrium solution for a hybrid star. The star stabilizes again by a large quark matter core in the interior (Figure 3.3(d)). With reference to Chapter 1, we denote the stars of the second stable branch of neutron stars "third family" stars.

Figure 3.3: Schematic diagram of the four different possible kinds of mass-radius curves for hybrid stars. Pure hadron stars are characterized by a blue line, hybrid stars by a red line. Stable star configurations are presented with a continuous line, unstable with a dashed line. In contrast to (b) and (c), the stars in (a) and (d) are destabilized immediately by the occurrence of a small quark core. For cases (b) and (d) we can find a stable quark branch after a destabilized one. We call these stars "third family" stars.

In contrast to the two previous types, stars of type **(C)** "**Connected**" will not be destabilized immediately after the phase transition. But as soon as the star is destabilized, it will not stabilize again by larger quark cores (Figure 3.3(c)). The larger the transition pressures P_{pt}, the smaller is the connected hybrid star branch. The branch can even be so small that it could not be seen by the used enlargement window in Figure 3.3(c).

The fourth case "**Both**" **(B)** (connected and disconnected) behaves like case C directly after the phase transition. In contrast to C, the star stabilizes again after an unstable hybrid star branch. We can find "third family" stars in this case. The "Both" case is shown in Figure 3.3(b) and the length of its connected hybrid star branch is in general very short.

With reference to criterion (3.22), the energy density discontinuity $\Delta\epsilon$ of case A or D must be chosen above the critical value $\Delta\epsilon_{\text{crit}}$.

3.3.2 "Phase" diagram for fixed hadronic EoS and quark matter sound velocity

The occurrence of the four different types of MR curves with respect to the parameters $P_{\text{pt}}/\epsilon_{\text{pt}}$ and $\Delta\epsilon/\epsilon_{\text{pt}}$ is shown in Figure 3.4. "Third family" stars appear in the MR types B and D.
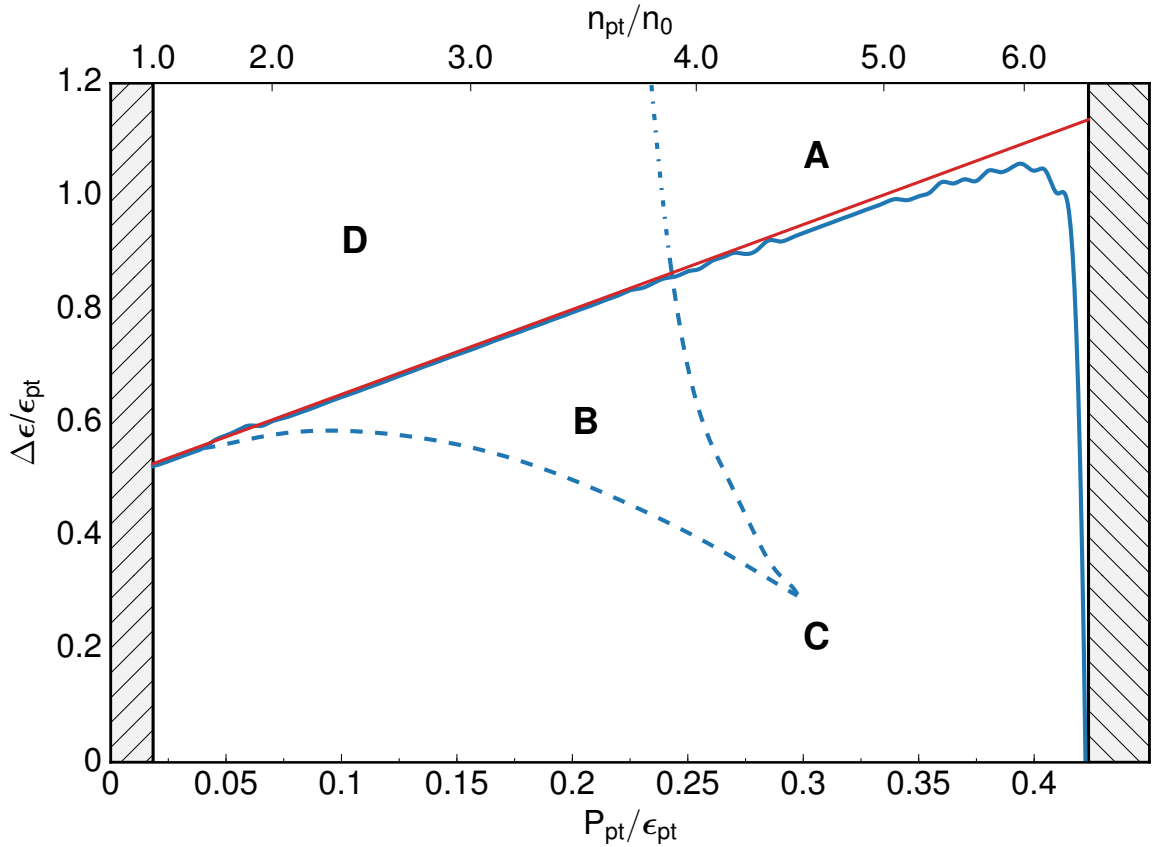
Figure 3.4: The "phase" diagram of MR curves with the BHF(N,l) EoS and $c_{\text{QM}}^2 = 1$ depending on the proportions $\Delta\epsilon/\epsilon_{\text{pt}}$ and $P_{\text{pt}}/\epsilon_{\text{pt}}$. The solid red line denotes the stabilization criterion (3.22). The shaded area at low densities ($n_{\text{pt}} < n_0$) is excluded since no phase transition could be observed in nuclear matter. The hatched area at high densities is excluded because the transition pressure P_{pt} is above the central pressure of the heaviest pure hadronic star P_{max}.

To compute this diagram, we vary the transition parameters P_{pt} and $\Delta\epsilon$ over a wide range and calculate the corresponding mass-radius curves. This leads to some kind of a grid consisting of mass-radius relations. By classifying the MR relations, with respect to one of the four types

described in Section 3.3.1, we can divide this grid into different parts A, B, C and D. To reach a "high" resolution of this "phase" diagram, we calculate up to 2500 MR curves, each consisting of about 350 different central pressure stars, which will be again calculated in up to 1000 steps.

The shown "phase" diagram 3.4 characterizes the occurrence of the four different mass-radius types separated by various blue lines. A phase transition from the hadronic BHF(N,l) to the quark CSS EoS with $c_{QM}^2 = 1$ is assumed. Two hatched areas are excluded from the observation. At small pressures (where $n_{pt} < n_0$) the phase transition would even occur in nuclear matter. Since no phase transitions to quark matter could be observed below the saturation density, we exclude this area. The hatched band at high pressures represents pressures above the maximal central pressure of a stable hadronic star P_{max}. The phase transition would occur in unstable equilibrium solutions. Since we could not find any signs that a transition to quark matter could stabilize the star again, we exclude this area as well.

The criterion (3.22) for small stable quark cores is marked by the solid red line. It reproduces the border of connected and disconnected hybrid branches (blue solid line) over a wide range of pressures. Below the solid blue line, the stable quark branch is connected (B and C) with the hadron branch, above it is disconnected (A and D). The fluctuations of our calculated line can be explained by numerical uncertainties. If we consider high pressures (near P_{max}) the deviation between the two lines increases enormously. We suppose two possible reasons for this fact: First the calculation is incorrect due to numerical issues and second the approximative derivation of Equation (3.22) is not valid anymore. Since there is no reason why the approximation becomes invalid at higher pressure values outside the infinitesimal vicinity of P_{max}, we exclude this possibility. Nevertheless it would be interesting to know, how criterion 3.22 would change, if we use more terms in the approximation of Equation (3.13) and (3.16). This task will be left out for work in the future. The reason for numerical issues can be explained as follows: The maximum of the MR curve represents a reversal point. Close to this maximum we have to choose very small central pressure steps to detect an increasing curve. Since the resolution of mass and radius between two stars with evanescently different central pressures is bordered by numerical uncertainties, we can not reproduce the vanishingly small stable hybrid branch. Therefore these stars are classified as "Absent".

Both the dashed and dashed-dotted blue line represent the transition where the second hybrid branch appears/disappears. Referring to Figure 3.5, we will discuss the evolution of the MR curves for increasing energy density discontinuity $\Delta\epsilon$ at fixed $P_{pt}/\epsilon_{pt} = 0.22$. We start from the blue ($\Delta\epsilon/\epsilon_{pt} = 0.1$) connected case and increase $\Delta\epsilon$. In the connected hybrid branch a point of inflection appears. This leads to a disconnected branch while crossing the dashed line (red line in Figure 3.5 with $\Delta\epsilon/\epsilon_{pt} = 0.5$). In contrast to the old branch, the star masses decrease, the minimal radius of a stable star decreases as well and the maximal central pressure of a stable star increases. This trend of the behavior of the three properties continues with increasing energy density discontinuity. While crossing into region D, the stable connected hybrid branch disappears (green line $\Delta\epsilon/\epsilon_{pt} = 1.0$). The mass and radius of the stable star with the maximal central pressure decrease further.

Crossing the dashed or dashed-dotted line of Figure 3.4 by decreasing the transition pressure P_{pt} a stationary point of inflection appears at the central pressure $P_{ip} > P_{pt}$. Therefore a new

disconnected branch originates with a new maximum-minimum pair. If we further decrease P_{pt}, the maximal mass of the disconnected branch increases and the minimal radius decreases.

Since P_{pt}/ϵ_{pt} is a monotonically increasing function with respect to P_{pt}, we can reparametrize the "phase" diagram 3.4 depending on $\Delta\epsilon$ and P_{pt} (Figure 3.6). Regarding the allocation of the four MR types, we can say that at low transition pressures case C occurs for low $\Delta\epsilon$ and case D for high energy density discontinuities. To obtain case B, the parameters have to be chosen very specific and the total area is small compared to the other cases. For high transition pressures, the star is more robust against changes of the energy density discontinuity and only destabilizes at very high $\Delta\epsilon$.
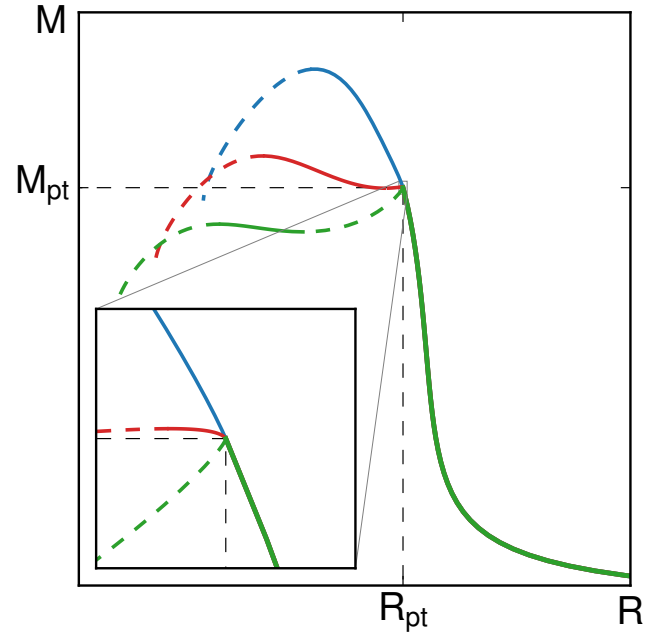
Figure 3.5: The evolution of MR curves on the "phase" diagram (Figure 3.4), for fixed $P_{pt}/\epsilon_{pt} = 0.22$ and increasing $\Delta\epsilon/\epsilon_{pt}$ (blue line: $\Delta\epsilon/\epsilon_{pt} = 0.1$, red line: $\Delta\epsilon/\epsilon_{pt} = 0.5$, green line: $\Delta\epsilon/\epsilon_{pt} = 1.0$). Solid lines represent stable star configurations, dashed lines unstable ones.

Due to this allocation of the four different cases we obtain the following conditions for the occurrence of "third family" stars: The phase transition to quark matter occurs at relatively small ($P_{pt} \lesssim 200\,\mathrm{MeV\,fm^{-3}}$) transition pressures and high energy density discontinuities $\Delta\epsilon \gtrsim 200\,\mathrm{MeV\,fm^{-3}}$. The corresponding transition baryon density is lower than $4n_0$. This would fit to the assumption, that a phase transition to quark matter occurs at particle densities of $2n_0 \lesssim n \lesssim 4n_0$ [2, 9]. Therefore an observation of a "third family" star could give a sign to confirm the assumed phase transition from hadronic matter to quark matter. Moreover an observation could possibly provide information about the transition parameters. In Chapter 4 we will analyze how the occurrence of the "third family" stars will change, if we give up the assumption of a sharp first-order phase transition and use a continuous crossover.

The physical understanding behind the allocation of the four types is as follows:
Due to the larger densities of the quark phase, a phase transition in the interior of a star causes an additional gravitational pull on the star. With rising energy density discontinuity this pull will increase as well. At low transition pressures the hadronic mantle is not robust enough to counteract large gravitational pulls. Hence the connected hybrid branch vanishes already at low $\Delta\epsilon$. If this happens, a larger quark core at higher central pressures (and smaller radius R_{NS}) can sustain the hadronic mantle and will stabilize the star again. A disconnected branch appears. At higher transition pressures the hadronic mantle is more massive and therefore more stable against a gravitational pull caused by the quark core. To eliminate the connected branch, the necessary $\Delta\epsilon$ is much larger. If this happens, the hadronic mantle is so heavy that even large quark cores can not sustain it and no hybrid star is stable at all (even at higher pressures and

smaller radii). Since increasing the energy density discontinuity makes the quark core heavier and increases the gravitational pull, the star will be destabilized at a certain point for fixed P_{pt}. Therefore the negative slope of the dashed-dotted line is explainable. The occurrence of case B is more complicated and can not be explained intuitively [43]. In the connected branch the pressure balances the increased gravitational pull caused by the phase transition. With increasing central pressure, the star is destabilized first and somehow stabilizes again at higher central pressures. A further discussion of this should be part of following work.
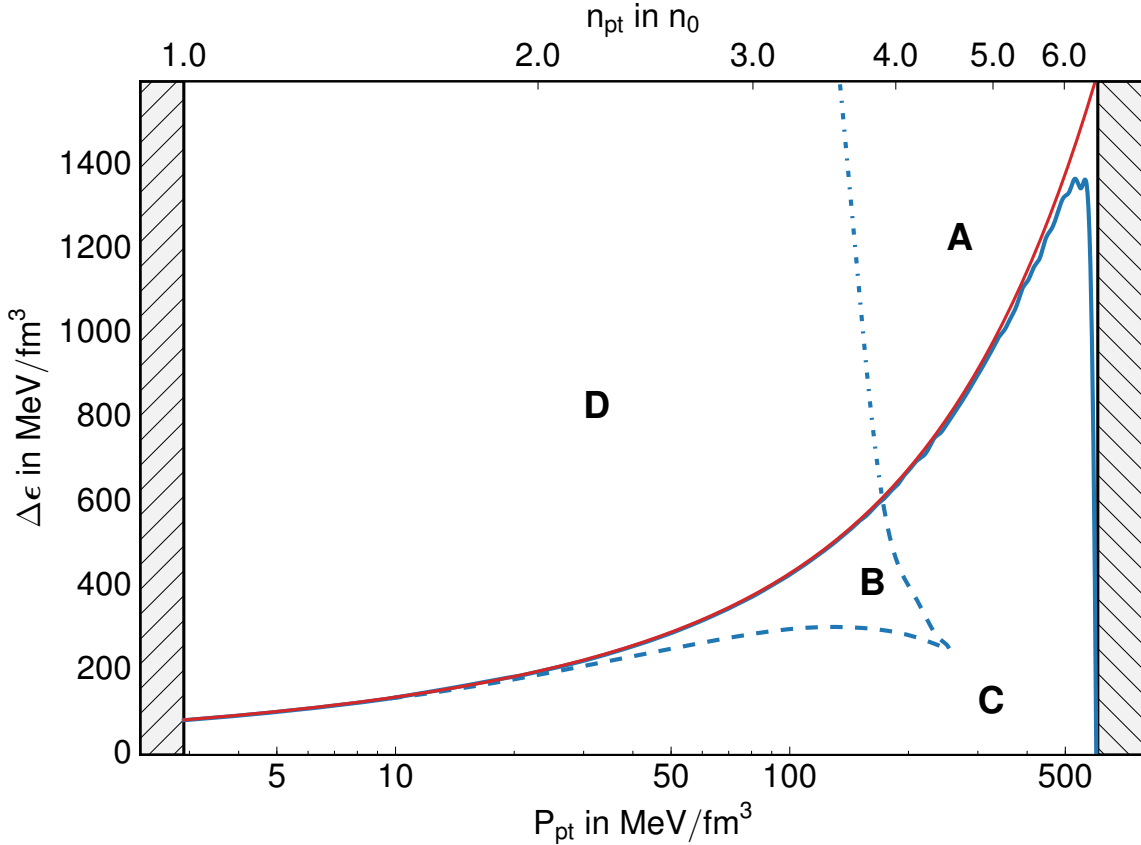
Figure 3.6: The "phase" diagram of MR curves with the BHF(N,l) EoS and $c_{QM}^2 = 1$ depending on $\Delta\epsilon$ and P_{pt}. The solid red line denotes the stabilization criterion (3.22). The shaded area at low densities ($n_{pt} < n_0$) is excluded since no phase transition could be observed in nuclear matter. The hatched area at high densities is excluded because the transition pressure P_{pt} is above the central pressure of the heaviest pure hadronic star P_{max}.

The "phase" diagrams for the two different hadronic EoSs (BHF(N,l) and χSU(3)) and the two sound velocities ($c_{QM}^2 = 1$ and $c_{QM}^2 = 1/3$) are shown in Figure 3.7. We will now discuss the effect of varying $\epsilon_{HM}(P)$ and c_{QM}^2 and explain its physical background:

As mentioned in Section 2.4.2, the BHF(N,l) EoS is stiffer than the χSU(3) EoS. For χSU(3) the maximal central pressure for stable hadronic stars P_{max} is reached at lower pressures. Therefore its maximal value of P_{pt}/ϵ_{pt} is not as high as the ones of BHF(N,l). The deviation of the solid lines (border between A/D and B/C) to the criterion (3.22) (red line) does not depend on the EoS and can be explained as in Section 3.3.2. The allocation of the four regions is quite sensitive to changes of the hadronic EoS and the quark EoS. Varying the equation of state to a softer one, the "Both" region consisting of a connected and disconnected branch, nearly reaches to $\Delta\epsilon/\epsilon_{pt} = 0$ at high transition pressures. For the χSU(3) EoS and $c_{QM}^2 = 1$ with a given transition pressure (here: $P_{pt}/\epsilon_{pt} \approx 0.25$), a disconnected "third family" branch appears even for low energy density discontinuities $\Delta\epsilon/\epsilon_{pt} \approx 0.03$. The gravitational pull of a large quark core with high transition pressure can be balanced by the softer hadronic mantle. Decreasing the sound velocity c_{QM}^2 will especially shift the dashed-dotted line (border between A and D) and dotted line (border between B and C) to lower transition pressures. For lower sound velocities $c_{QM}^2 = dP/d\epsilon$, the energy density increases faster with increasing pressure. Therefore the gravitational pull increases at high pressures of large quark matter cores and the star tends to destabilize. This shifts the border of stable "third family" stars to lower transition pressures.
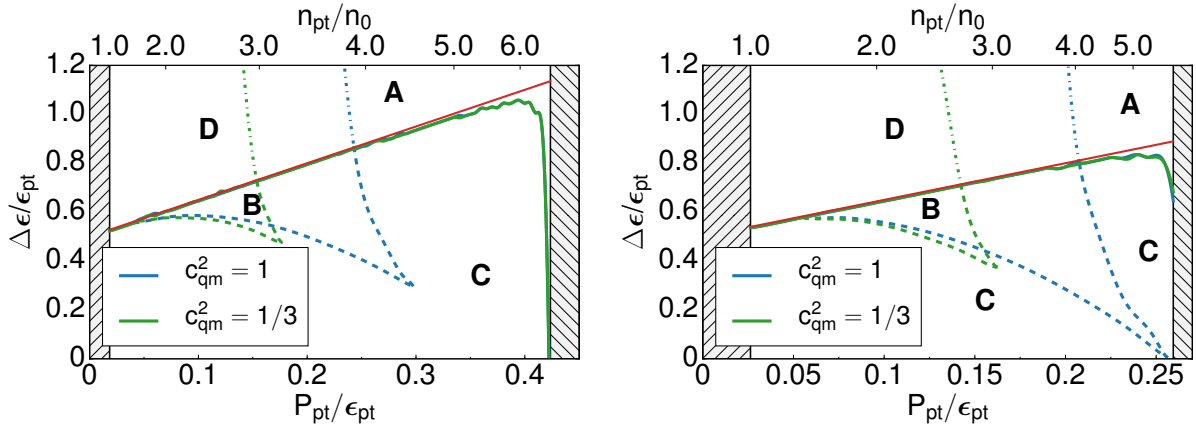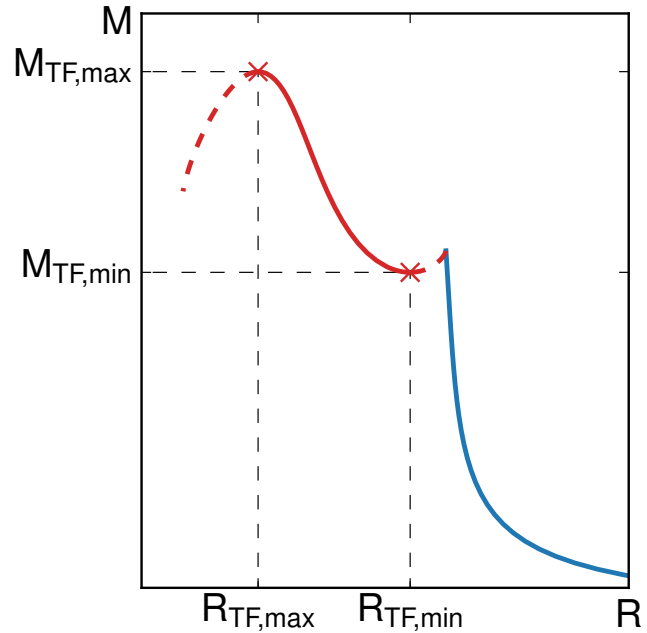

(a) "Phase" diagram for the BHF(N,l) EoS.   (b) "Phase" diagram for the χSU(3) EoS.

Figure 3.7: The dependency on the "phase" diagram on different EoSs. In (a) the diagram is computed using the hadronic BHF(N,l) EoS, in (b) using the χSU(3) EoS. The blue lines denote the "phase" diagram for the sound velocity $c_{QM}^2 = 1$, the green lines for $c_{QM}^2 = 1/3$. The red line denotes the stabilization criterion (3.22). The hatched area at low densities ($n_{pt} < n_0$) is excluded since no phase transition could be observed in nuclear matter. The shaded band at high densities is excluded because the transition pressure P_{pt} is above the central pressure of the heaviest pure hadronic star P_{max}. Respect the different scaling of the P_{pt}/ϵ_{pt} axis in (a) and (b).

## 3.4 Observables of "third family" compact stars

In this section we want to find out which radii and masses "third family" stars have. Therefore we denote the "third family" star with maximal stable mass of one MR curve TF_{max} (with $(R, M)_{NS} = (R, M)_{TF,max}$). The corresponding "third family" star with minimal stable mass is denoted by TF_{min} (with $(R, M)_{NS} = (R, M)_{TF,min}$). This notation is visualized with the help of a MR curve in Figure 3.8. Since the MR curve is monotonous, the values of the masses and radii of all "third family" stars must be between the masses and radii of TF_{max} and TF_{min}. The exact values of the mass and radius of these two stars depend on the CSS parametrization. Therefore we will analyze these two stars on the "phase" diagram for different hadronic EoSs and quark matter sound velocities. Due to this we are able to specify the "third family" radii of the observed neutron star masses.

In Figure 3.9 contour plots of the minimal mass of "third family" stars are shown depending on the hadronic EoS, the quark matter sound velocity c_{QM}^2 and the transition

Figure 3.8: Schematic of a MR curve with a "third family" branch. Red lines denote hybrid stars, blue lines hadronic stars. Solid lines represent stable star configurations, dashed lines unstable ones. The two "third family" stars TF_{max} and TF_{min}, with the maximal and minimal mass are marked with a cross.

parameters P_{pt}, $\Delta\epsilon$. Their associated radii are shown in Figure 3.10. The maximal masses and the corresponding radii of "third family" compact stars are shown in Figure 3.11 and 3.12. For the upper row of the four figures, the stiffer BHF(N,l) EoS is used for the hadronic matter and for the lower row the softer χSU(3) EoS. The left plots represent contour plots using the quark matter sound velocity $c_{QM}^2 = 1$, the right ones $c_{QM}^2 = 1/3$. Due to the numerical issues described in Section 3.3.2, we use criterion (3.22) instead of the calculated border between the regions of connected (B, C) and disconnected (A, D) branches. This criterion is indicated by the solid red line. In each plot the border between the four MR types is visualized by a dashed/dashed-dotted blue line and the red line. The hatched area at low transition pressures ($n_{pt} < n_0$) is excluded since matter at saturation density consists of a pure hadronic phase. The shaded area at high transition pressures is excluded as well, since the transition pressure P_{pt} is above the maximal stable central pressure of a pure hadronic star P_{max} and no "third family" stars could be found.
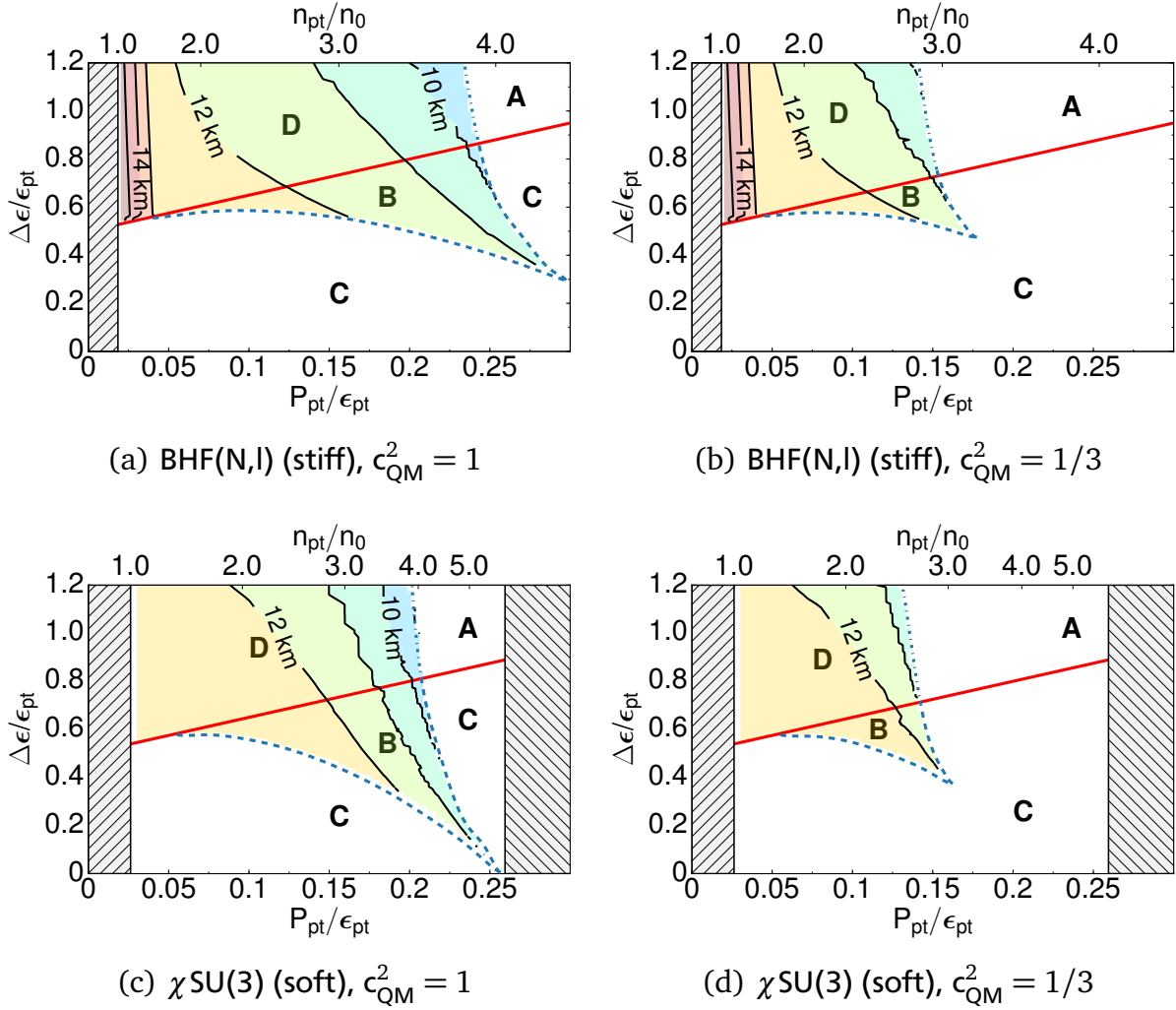
The minimal mass of "third family" stars $M_{TF,min}$ varies from $0.5\,M_\odot$ to $1.9\,M_\odot$. The mass increases with higher transition pressures and decreasing energy density discontinuity. In this process, the minimal mass is nearly independent of the hadronic equation of state, but reaches
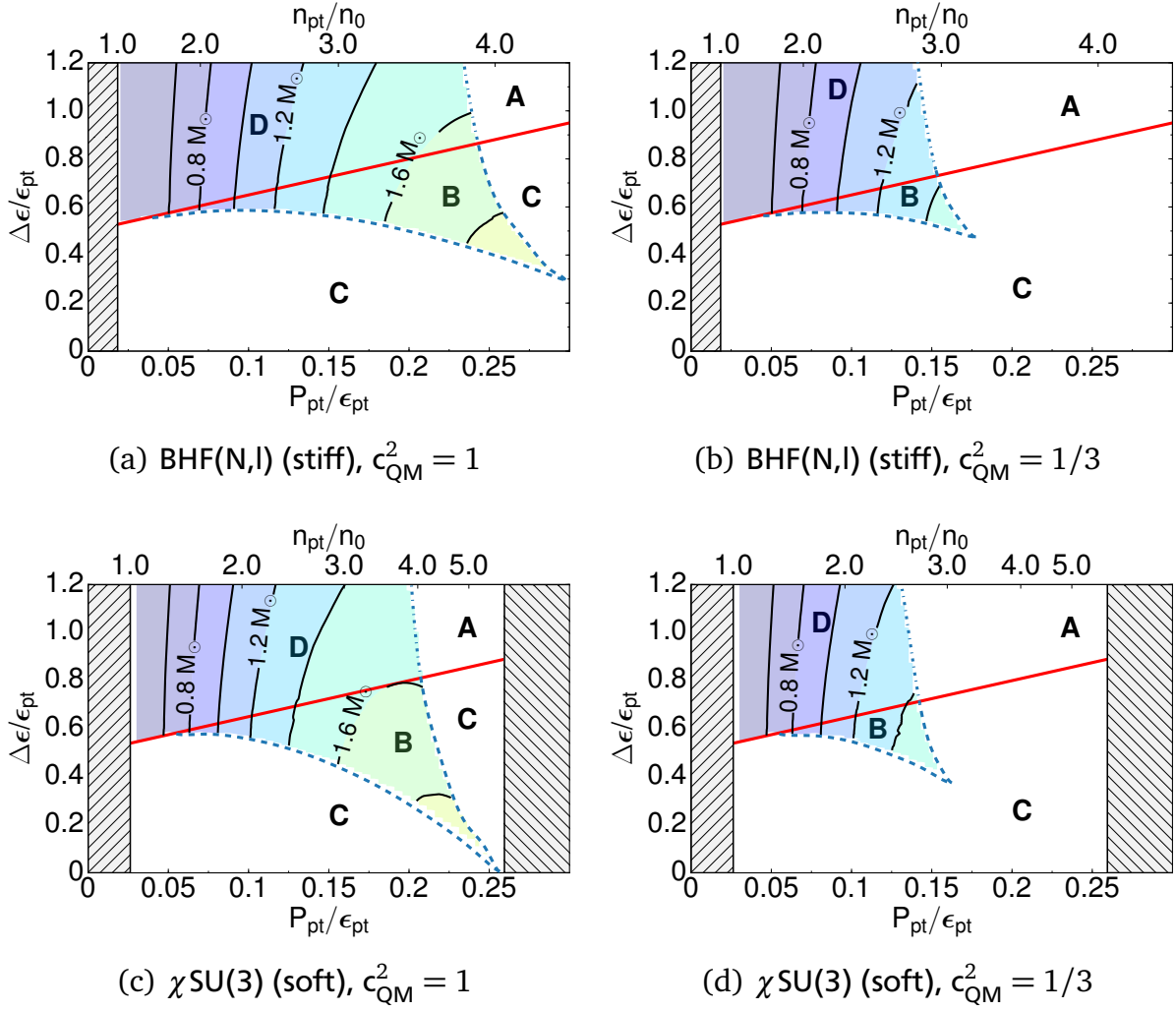
Figure 3.9: Contour plots visualizing the mass of TF_{min} as a function of the CSS parametrization. Each plot is shown above the corresponding "phase" diagram with the B,D region in detail. They depend on the transition parameters P_{pt}/ϵ_{pt}, $\Delta\epsilon/\epsilon_{pt}$ and n_{pt}/n_0. The hatched area at low densities ($n_{pt} < n_0$) is excluded since no phase transition could be observed in nuclear matter. The shaded band at high densities is excluded, because the transition pressure P_{pt} is above the central pressure of the heaviest pure hadronic star P_{max} and no "third family" stars could be observed for higher transition pressures. The red line denotes the stabilization criterion (3.22). For nuclear matter the BHF(N,l) EoS is used in the upper row and the χSU(3) EoS used in the bottom row. The plots (a) and (c) use the sound velocity $c_{QM}^2 = 1$ and the plots (b) and (d) use $c_{QM}^2 = 1/3$ for the quark matter EoS.

higher masses for increasing sound velocity. The corresponding radii $R_{TF,min}$ range from 9 km to 16 km. The higher P_{pt} and $\Delta\epsilon$, the smaller is the radius of the star. Contrary to the mass, the radius shows only a moderate dependency on the quark matter sound velocity. It is mainly determined by the hadronic EoS and can reach higher values for stiffer EoSs.

The values of the mass and radius of the quark matter core of TF_{min}, can reach up to $M_{TF,min,core} \approx 0.8\,M_\odot$ and $R_{TF,min,core} \approx 5$ km. The higher the transition pressure, the higher is the quark core mass. After increasing the $\Delta\epsilon$ at high P_{pt}, the core mass will rise enormously and will take more than 50 % of the star mass. At the same time the central particle density

(a) BHF(N,l) (stiff), $c_{QM}^2 = 1$

(b) BHF(N,l) (stiff), $c_{QM}^2 = 1/3$

(c) χSU(3) (soft), $c_{QM}^2 = 1$

(d) χSU(3) (soft), $c_{QM}^2 = 1/3$

Figure 3.10: Contour plots visualizing the radius of TF_{min} as a function of the CSS parametrization. Each plot is shown above the corresponding "phase" diagram with the B,D region in detail. They depend on the transition parameters P_{pt}/ϵ_{pt}, $\Delta\epsilon/\epsilon_{pt}$ and n_{pt}/n_0. The hatched area at low densities ($n_{pt} < n_0$) and high densities as well as the red line are defined as in Figure 3.9. For nuclear matter the BHF(N,l) EoS is used in the upper row and the χSU(3) EoS used in the bottom row. The plots (a) and (c) use the sound velocity $c_{QM}^2 = 1$ and the plots (b) and (d) use $c_{QM}^2 = 1/3$ for the quark matter EoS.

reaches up to $n_c \approx 10\,n_0$. The radius of the quark core rises as long as $\Delta\epsilon$ or P_{pt} increase. For this reason we will find the largest and heaviest quark cores in the interior of the smallest stars. The "third family" stars with the maximal stable mass TF_{max} have radii of 8 km to 14 km. In contrast to Figure 3.10, the smallest stars do not occur at the highest possible transition pressure, but in general the radii of TF_{max} and TF_{min} trend in the same way. However with reference to the mass, they behave completely different. The smaller P_{pt} and $\Delta\epsilon$, the larger is the mass of TF_{max}. In this context $M_{TF,max}$ differs from $1.3\,M_\odot$ to $2.9\,M_\odot$ and depends mainly on the quark matter sound velocity. The higher c_{QM}^2, the higher is the mass.

The quark core of TF_{max} behaves like its radius and mass. The core gets larger and heavier for low transition pressures. In this case the mass and radius of the quark core can reach values up to $M_{TF,max,core} \approx 2.5\,M_\odot$ and $R_{TF,max,core} \approx 10$ km. Therefore the principle part of the star consists
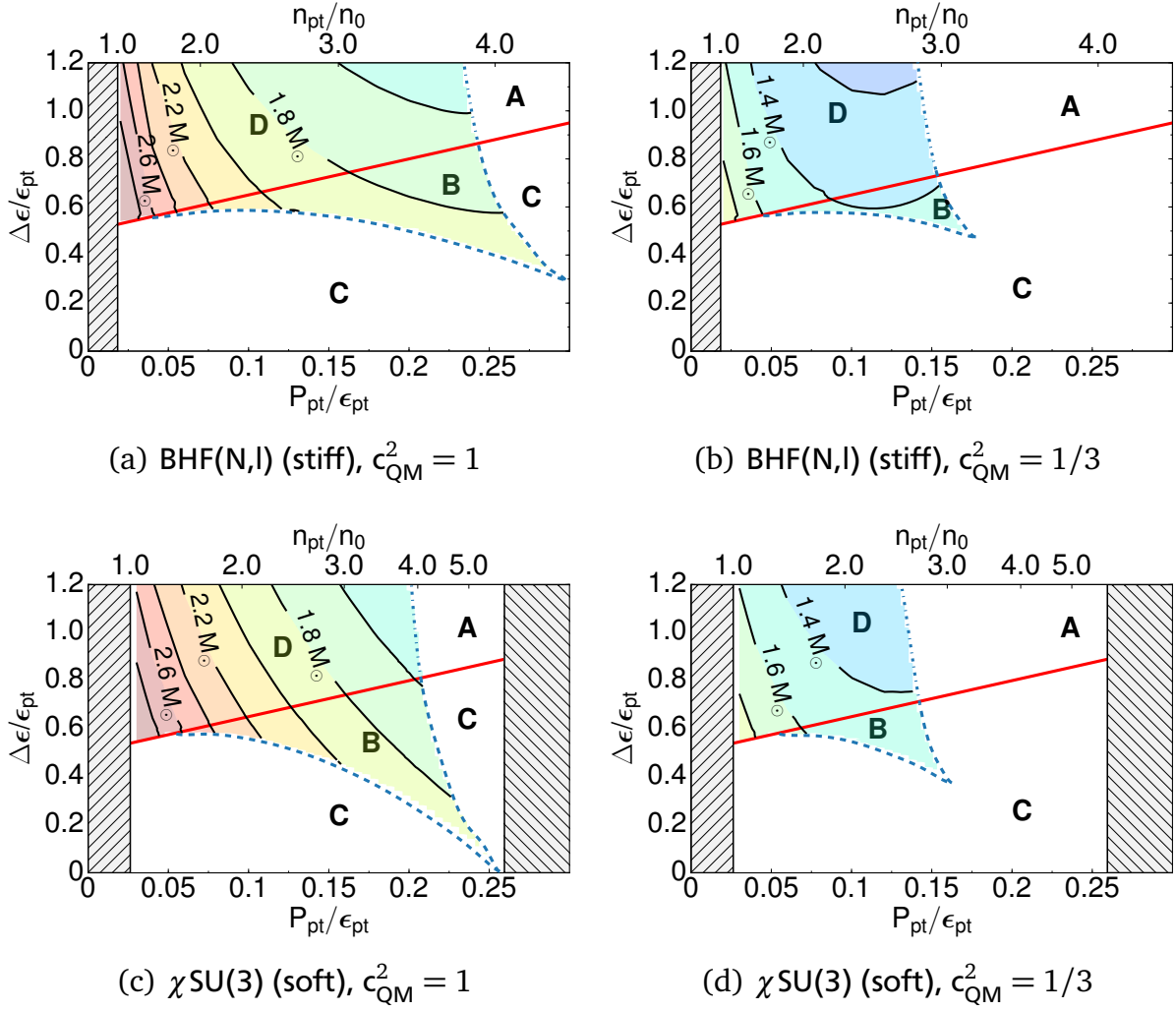
Figure 3.11: Contour plots visualizing the the mass of TF_{max} as a function of the CSS parametrization. Each plot is shown above the corresponding "phase" diagram with the B,D region in detail. They depend on the transition parameters P_{pt}/ϵ_{pt}, $\Delta\epsilon/\epsilon_{pt}$ and n_{pt}/n_0. The hatched area at low densities ($n_{pt} < n_0$) and high densities as well as the red line are defined as in Figure 3.9. For nuclear matter the BHF(N,l) EoS is used in the upper row and the χSU(3) EoS used in the bottom row. The plots (a) and (c) use the sound velocity $c_{QM}^2 = 1$ and the plots (b) and (d) use $c_{QM}^2 = 1/3$ for the quark matter EoS.

of quark matter. The quark core is nearly independent of the hadronic EoS, but its mass increases a lot with rising c_{QM}^2.

For realistic CSS parameters (sound velocity based on the asymptotic freedom $c_{QM}^2 = 1/3$ and transition particle density of $2n_0 \lesssim n \lesssim 4n_0$) and the used hadronic EoSs, we recap for the radius R_{TF} and mass M_{TF} of "third family" stars

$$9\,\text{km} \lesssim R_{TF} \lesssim 12\,\text{km}, \qquad\qquad 1.1\,M_\odot \lesssim M_{TF} \lesssim 1.5\,M_\odot. \qquad (3.23)$$

Since mass and radius are not independent, not all star configurations of Equation (3.23) are possible. Nevertheless we should be skeptical about this outcome.
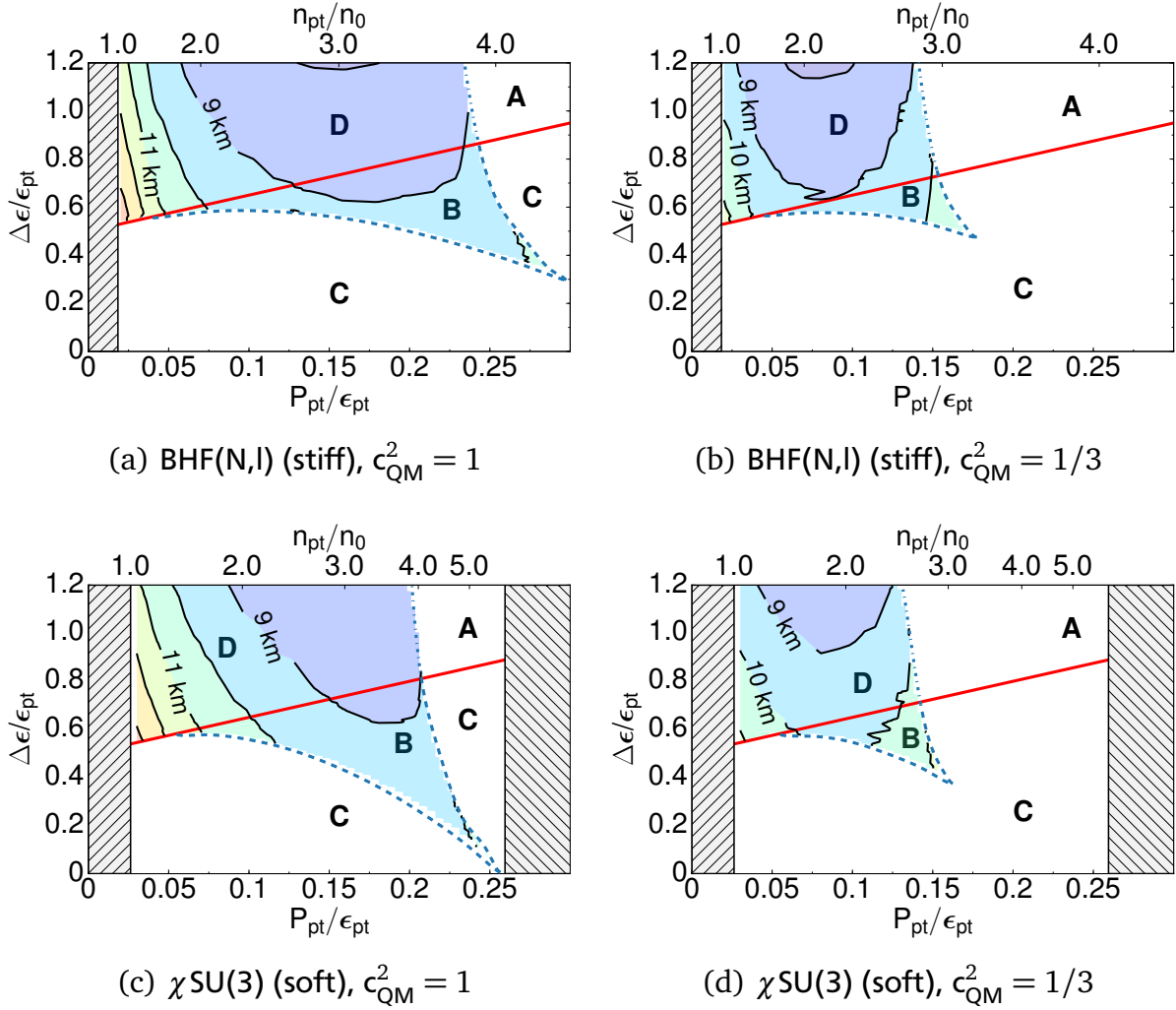
Figure 3.12: Contour plots visualizing the the radius of TF_{max} as a function of the CSS parametrization. Each plot is shown above the corresponding "phase" diagram with the B,D region in detail. They depend on the transition parameters P_{pt}/ϵ_{pt}, $\Delta\epsilon/\epsilon_{pt}$ and n_{pt}/n_0. The hatched area at low densities ($n_{pt} < n_0$) and high densities as well as the red line are defined as in Figure 3.9. For nuclear matter the BHF(N,l) EoS is used in the upper row and the χSU(3) EoS used in the bottom row. The plots (a) and (c) use the sound velocity $c_{QM}^2 = 1$ and the plots (b) and (d) use $c_{QM}^2 = 1/3$ for the quark matter EoS.

The "third family" stars could only attain masses up to $1.5\,M_\odot$, which means that they can not describe the recently observed supermassive neutron stars with masses of $M_{NS} \approx 2.0\,M_\odot$. Even for pure hadronic stars, which are described by the hadronic part of these hybrid EoSs, the maximal masses are not significant larger than $1.5\,M_\odot$. Therefore the chosen EoSs probably do not describe real neutron/"third family" stars. Nevertheless we want to outline a further consequence of our calculations. The mass of the Hulse-Taylor pulsar fits in the calculated range of "third family" stars. If we assume that this pulsar would be a "third family" star, then our calculations would lead to a radius between $9.5\,km$ and $12.5\,km$.
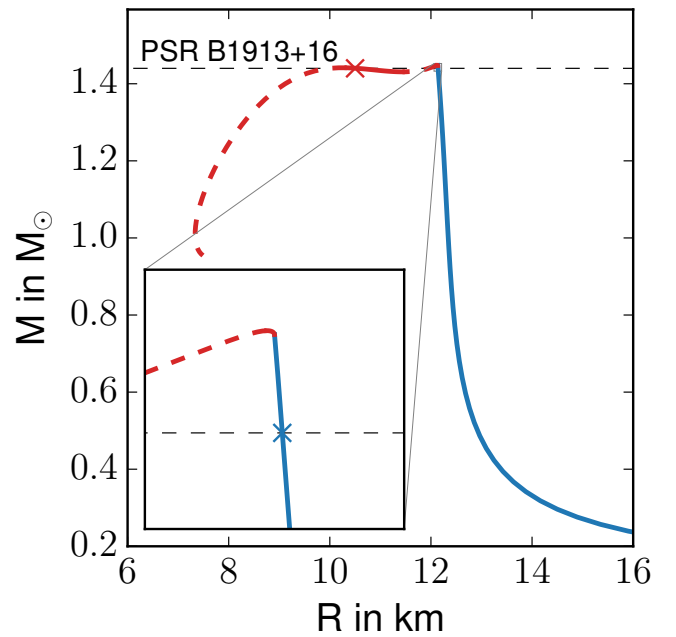
3.5 "Neutron star twins"

In the previous section we analyzed possible masses of "third family" stars, which match with typical neutron star masses. Since the neutron star branch will abort, due to a decrease of mass, we will find a mass regions where the "third family" stars and neutron stars overlap. We denote the non-identical stars (one neutron star and one "third" family star) with the same masses "neutron star twins". In the following, the structure of these "neutron star twins" will be compared. Furthermore we discuss why the dicovery of "neutron star twins" is a possible signature for phase transitions.

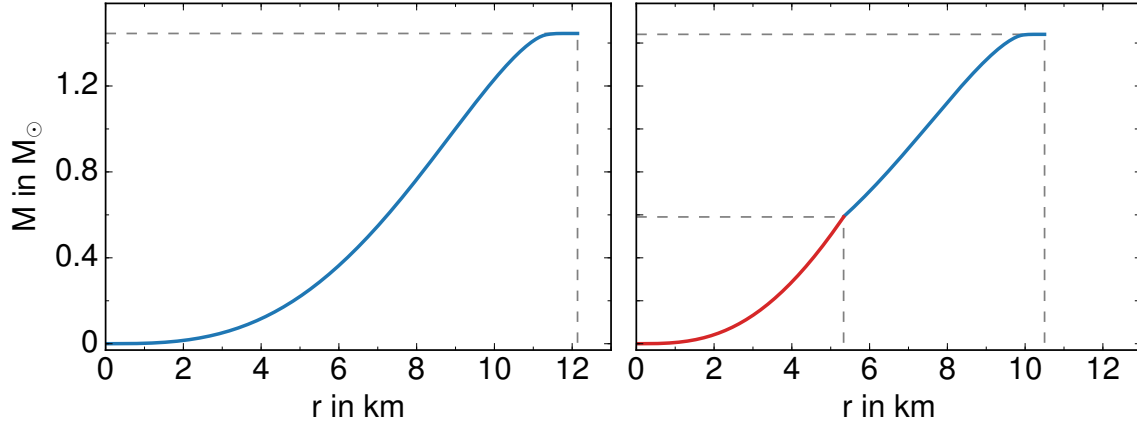### 3.5.1 The structure of "neutron star twins" in comparison

We will now analyze the structure of a "third family" star and compare it to its neutron star counterpart with the same mass as the Hulse-Taylor pulsar. To achieve this, we choose the BHF(N,l) EoS, the CSS value $c_{QM}^2 = 1/3$ and a MR curve in the region B with the transition parameters $P_{pt}/\epsilon_{pt} = 0.155$ ($P_{pt} = 79.84\,\mathrm{MeV\,fm^{-3}}$) and $\Delta\epsilon/\epsilon_{pt} = 0.6$ ($\Delta\epsilon = 309.04\,\mathrm{MeV\,fm^{-3}}$). The corresponding mass-radius curve is shown in Figure 3.13. The stars with a mass of $M = 1.44\,M_\odot$ are marked as a cross and differ in their radii by values of $R_{NS} = 12.14\,\mathrm{km}$ (neutron star) and $R_{TF} = 10.5\,\mathrm{km}$ ("third family" star). While the "third family" star contains a quark matter core, the central pressure of the neutron star is not high enough for a phase transition. Therefore it only consists of hadronic matter. In the following the two stars will be compared regarding the properties mass, pressure, energy density and particle density:

Figure 3.13: The MR curve of the a "Both" case with $P_{pt}/\epsilon_{pt} = 0.155$, $\Delta\epsilon/\epsilon_{pt} = 0.6$ and used BHF(N,l) EoS and CSS value $c_{QM}^2 = 1/3$. The two stars with the Hulse-Taylor pulsar mass are marked as a cross. Red lines denote hybrid stars, blue lines pure hadronic stars. Solid lines represent stable star configurations, dashed lines unstable ones.

The allocation of the mass is shown in Figure 3.14. We can see that the principle part of the neutron star mass is caused by the matter between radii of 4 to 10 km. The mass of the crust is negligible. In contrast to this the quark core of the "third family" accounts for half of the star mass ($M = 0.59\,M_\odot$) within the first 5.33 km. This causes an immense gravitational pull.

This gravitational pull is visible in form of the central pressure in Figure 3.15(a). While the pressure of the ordinary neutron star only increases to $P_c = 79.38\,\mathrm{MeV\,fm^{-3}}$, the central pres-

Figure 3.14: The included mass M(r) as a function of the radius r. On the left the graph of the neutron star is shown. We compare this with the "third family" star on the right, containing a quark matter core (red line). The blue lines indicate the hadronic phase. Both stars have the same mass as the Hulse-Taylor pulsar ($M = 1.44\,M_\odot$) but differ in their radii $R_{NS} = 12.14\,\text{km}$, $R_{TF} = 10.5\,\text{km}$.

sure of the hybrid star reaches $P_c = 297.15\,\text{MeV fm}^{-3}$. The high values of the pressure at the quark phase correspond to high energy (Figure 3.15(b)) and particle densities (Figure 3.15(c)). They reach up to a multiple of the corresponding neutron star densities. The discontinuity of these two densities at the transition pressure increases the deviation even more.

Conversely we can argue that the energy density discontinuity of a first-order phase transition leads to a jump discontinuity of the included mass gradient at the phase transition. This fact is visualized in Figure 3.14. The gradient changes from a higher value at the quark matter to a lower value at the hadronic matter. Larger mass gradients lead to larger included masses, which induces a higher gravitational pull.
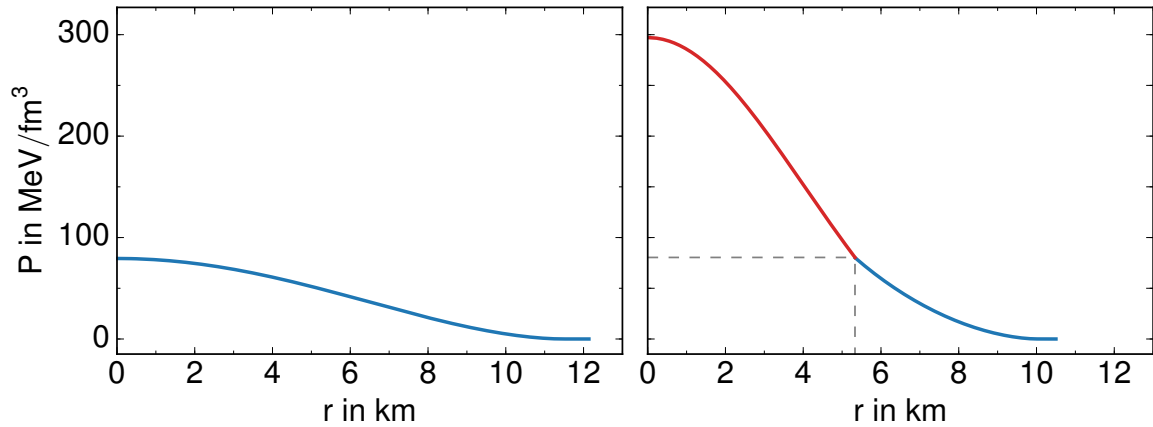
(a) The radial trend of the pressure of the two stars.
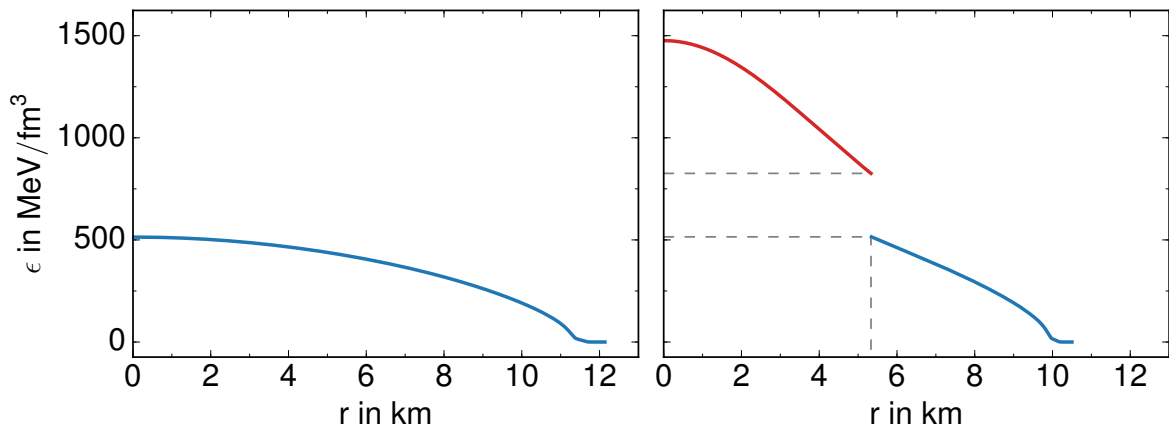
(b) The radial trend of the energy density of the two stars.
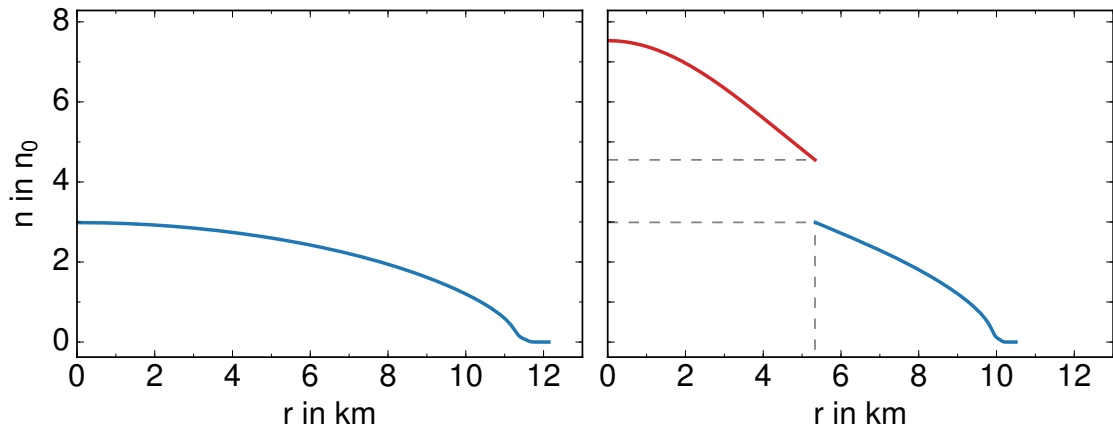
(c) The radial trend of the particle density of the two stars.

Figure 3.15: Pressure, energy density and particle density as a function of radius r in the interior of a star. The hadronic neutron star (left) and the corresponding quantities for the "third family" star (right) are compared. Both stars have the same mass as the Hulse-Taylor pulsar ($M = 1.44 \, M_\odot$) but differ in their radii $R_{NS} = 12.14 \, \text{km}$, $R_{TF} = 10.5 \, \text{km}$. Red lines denote quark matter, blue lines hadronic matter.

3.5.2 "Neutron star twins" as a possible signature for phase transitions

Due to the diversity of possible EoSs, the measurement of the observables of a single star do not provide enough information to classify it as a "third family" star or an ordinary neutron star. However the observation of "neutron star twins" do provide enough information to classify them. To explain this, we consider two neutron stars with a small deviation in mass ΔM and a large difference in radius ΔR (with $\Delta R \gg \Delta M$) and denote such a pair "quasi twin". The MR curves of typical neutron stars (Figure 2.7) do not provide a large difference in radius between two stars with nearly the same mass. A small modification in mass will only lead to a small change in radius ($\Delta M \approx \Delta R$). If we choose a "third family star" and neutron star with nearly the same mass, the radius of the two stars differ a lot ($\Delta R \gg \Delta M$). Therefore finding a quasi twin will automatically lead to the existence of a "third family" branch, since this is the only possible reason for the large difference in radius [1]. In this process the "neutron star twins" are only a special case of quasi twins. If we consider the "neutron star twins" of Section 3.5.1 ($\Delta R = 1.64\,\mathrm{km}$), the deviation in mass must be much less than $\Delta M = 1.11\,\mathrm{M_\odot}$ (obtained by the geometrized unit system) to satisfy the quasi twin condition ($\Delta R \gg \Delta M$). Since the masses of the "neutron star twins" are equal, this relation is satisfied.

With reference to Chapter 1, we know that for the existence of a third stable sequence of compact objects, the EoS must provide a sufficiently large discontinuity in the speed of sound (Gerlach's necessary condition). In previous sections and in [15] it is established that a phase transition to a deconfined quark matter can satisfy this condition and leads to "third family" stars. Even if it is not proven that this phase transition is the only reason for a third stable branch, it is maybe the most plausible one [12]. Hence the observation of rising twins is a possible signature for the deconfinement phase transition.

4 "Third family" stars and hadron-quark crossovers

In the previous chapter we have seen, that a first-order phase transition can lead to "third family" stars. In this chapter we debate whether a sharp first-order phase transition is the only possibility to obtain "third family" stars. For this reason the sharp phase transition will be smoothed by using a continuous interpolation between the two phases. We use a crossover which can be parametrized in different ways. Therefore we firstly discuss the used parametrization, which depends on the pressure crossover region Γ_P. Again, different transition parameter lead to the four MR types. We will reconstruct the known "phase" diagram with the crossover equation of state and analyze its dependency on Γ_P. From this we can discuss necessary conditions of the phase change for the occurrence of "third family" stars.

4.1 The crossover parametrization

First of all we want to shortly present the physical concept of this interpolation introduced in [9]. In the transition region between the hadronic phase and the deconfined phase, the state of the system can neither be described by an extrapolation of the hadronic equation of state for higher pressures, nor by extrapolating the quark EoS for lower pressures. Therefore we somehow connect the hadron EoS and the quark EoS by a continuous interpolation in the transition region Γ_P. In this work we use a crossover EoS, which means that the hadron phase and the quark phase will coexist. The higher the pressure, the higher is the total number of particles in the quark phase. In the style of [9] we use the following method to construct the crossover EoS:

$$\epsilon_{\mathrm{Cross}}(P) = \epsilon_{\mathrm{HM}}(P)\,f_-(P) + \epsilon_{\mathrm{QM}}(P)\,f_+(P), \qquad (4.1)$$

with the hadronic EoS ϵ_{HM}, the quark matter EoS ϵ_{QM} and the interpolation function $f_\pm$ with

$$f_\pm(P) = \frac{1}{2}\left(1 \pm \tanh\left(4 \cdot \frac{P - \overline{P}}{\Gamma_P}\right)\right). \qquad (4.2)$$

$\overline{P}$ is the mean pressure value of the crossover region. This region is characterized by the window

$$P_{\mathrm{CH}} := \quad \overline{P} - \frac{\Gamma_P}{2} \quad \lesssim \quad P \quad \lesssim \quad \overline{P} + \frac{\Gamma_P}{2} \quad =: P_{\mathrm{CQ}}. \qquad (4.3)$$

The pressures P_{CH} and $P_{\mathrm{CQ}} = P_{\mathrm{CH}} + \Gamma_P$ at the border of the transition region represent points, which we can essentially classify by the hadron phase respectively the quark phase. The equation

of state $\epsilon_{\mathrm{Cross}}$ has to conform to the hadronic / quark EoS at these points. This fact is nearly guaranteed due to the definition of Equations (4.1 - 4.3). By using these equations, we obtain

$$\tanh\left(4\cdot\frac{P_{\mathrm{CH}}-\overline{P}}{\Gamma_{\mathrm{P}}}\right)=\tanh(-2)\approx-0.96\,,\quad\tanh\left(4\cdot\frac{P_{\mathrm{CQ}}-\overline{P}}{\Gamma_{\mathrm{P}}}\right)=\tanh(2)\approx0.96\,,\qquad(4.4)$$

$$\Rightarrow\quad\epsilon(P_{\mathrm{CH}})\approx0.98\,\epsilon_{\mathrm{HM}}(P_{\mathrm{CH}})+0.02\,\epsilon_{\mathrm{QM}}(P_{\mathrm{CH}})\approx\epsilon_{\mathrm{HM}}(P_{\mathrm{CH}})\,,\qquad(4.5)$$

$$\Rightarrow\quad\epsilon(P_{\mathrm{CQ}})\approx0.02\,\epsilon_{\mathrm{HM}}(P_{\mathrm{CQ}})+0.98\,\epsilon_{\mathrm{QM}}(P_{\mathrm{CQ}})\approx\epsilon_{\mathrm{QM}}(P_{\mathrm{CQ}})\,.\qquad(4.6)$$

In order to compare the crossover EoS (4.1) with the CSS parametrization introduced in Section 3.1.2, we define $P_{\mathrm{CH}}=P_{\mathrm{pt}}$. Therefore the crossover region extends from P_{pt} to $P_{\mathrm{pt}}+\Gamma_{\mathrm{P}}$. We use the same hadron EoSs and quark EoSs $(\epsilon_{\mathrm{QM}}=1/c_{\mathrm{QM}}^2(P-P_{\mathrm{pt}})+\epsilon_{\mathrm{pt}}+\Delta\epsilon)$ as before. Additional to the parameters of the CSS parametrization, the crossover parametrization depends on the crossover region parameter Γ_{P}. These two parametrizations are visualized in Figure 4.1. The crossover region is indicated by a green line and visualized by grey bars. Beyond the crossover region both parameterizations are essentially equal. In contrast to the first-order phase transition, the crossover EoS connects the hadron phase (blue lines) and quark phase (red lines) continuously. The chemical potential and particle density as a function of the pressure P can be derived by using the fundamental thermodynamical relations analogously to Section 3.1.3.
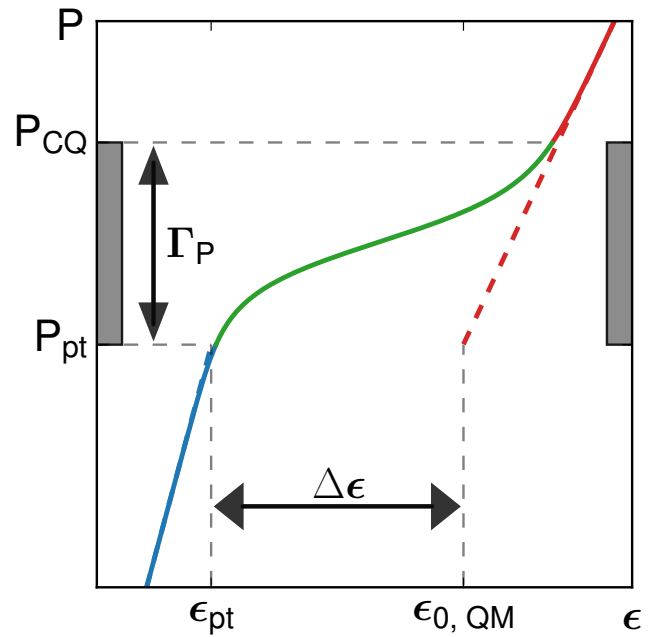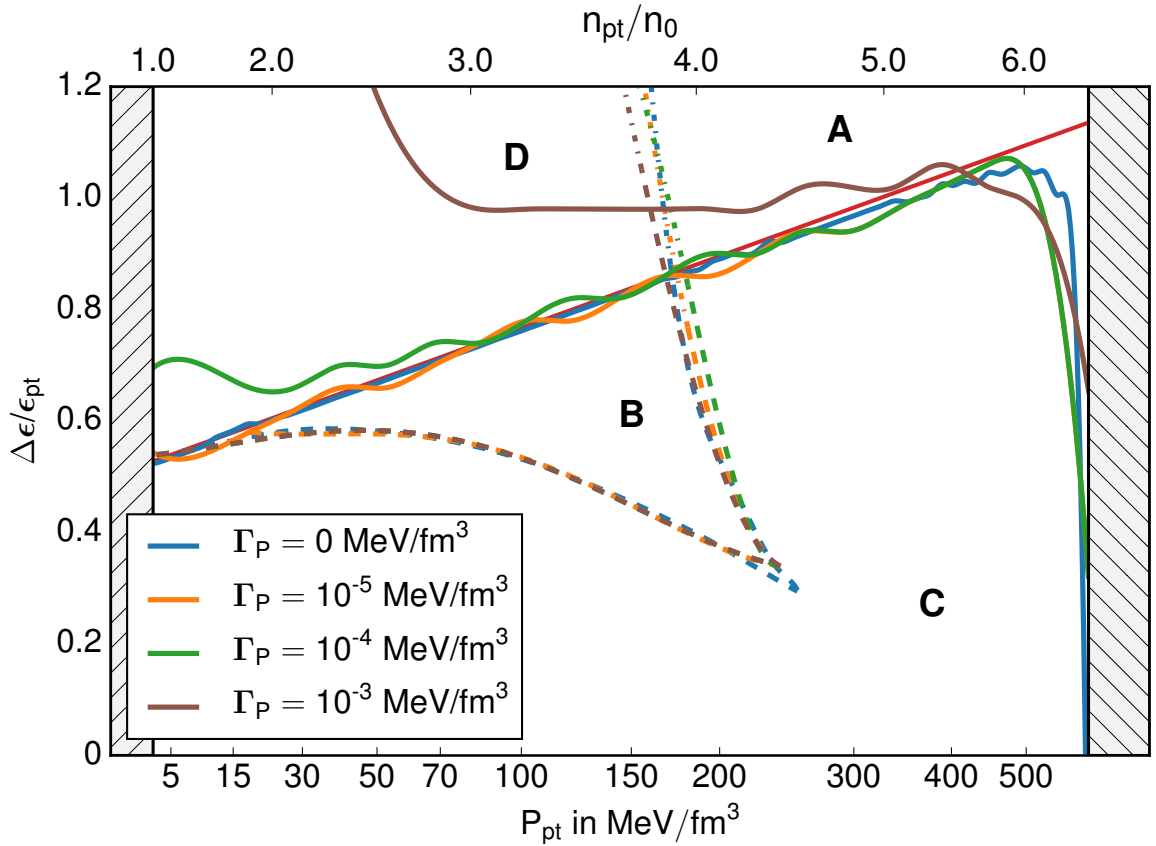

Figure 4.1: The CSS parametrization of Section 3.1.2 (dashed line) in comparison to the crossover parametrization (solid line) depending on the parameter P_{pt}, $\Delta\epsilon$ and Γ_{P}. The crossover region is indicated by a green line, the hadron/quark phase by blue/red lines.

In the context of a crossover, the pressure P_{CH} characterizes the point, where the system starts to transform into the quark matter phase. This transformation is essentially closed at the point P_{CQ}. For this reason we have to redefine the four MR types of Section 3.3.1. If a star is even destabilized by the occurrence of a small percentage of quark matter after the point P_{CH}, we classify it as A or D. The appearance of stable "third family" stars after a disconnected branch will again lead to the classification B or D. Since the central pressures $P_{\mathrm{TF,c}}\approx300\,\mathrm{MeV/fm^3}$ of "third family" stars is in general larger than the transition pressures of their occurrence ($P_{\mathrm{pt}}\lesssim100\,\mathrm{MeV/fm^3}$ for $c_{\mathrm{QM}}^2=1/3$) and the considered transition regions ($\Gamma_{\mathrm{P}}\leq100\,\mathrm{MeV/fm^3}$), we can assume that $P_{\mathrm{TF,c}}>P_{\mathrm{CQ}}$ holds. This leads to a pure quark matter core in the interior of "third family" stars.

4.2 "Phase" diagram of the crossover parametrization

After we introduced the crossover parametrization in the previous section, we will use this parametrization to analyze the occurrence of the four different MR types within the meaning of the crossover (Section 4.1). Analogously to Section 3.3.2, we calculate the MR curve for the different transition parameters P_{pt}, $\Delta\epsilon$, classify them to A, B, C or D and visualize these regions again in the known "phase" diagram. This procedure will be done for fixed hadronic EoS, c_{QM}^2 and various crossover regions Γ_P. For a further understanding of the used values of Γ_P, we show the "phase" diagram in dependency on P_{pt}, $\Delta\epsilon/\epsilon_{pt}$ and n_{pt}/n_0. Since the necessary time for computing increases enormously by using the crossover parametrization, we choose a slightly lower resolution of the grid.
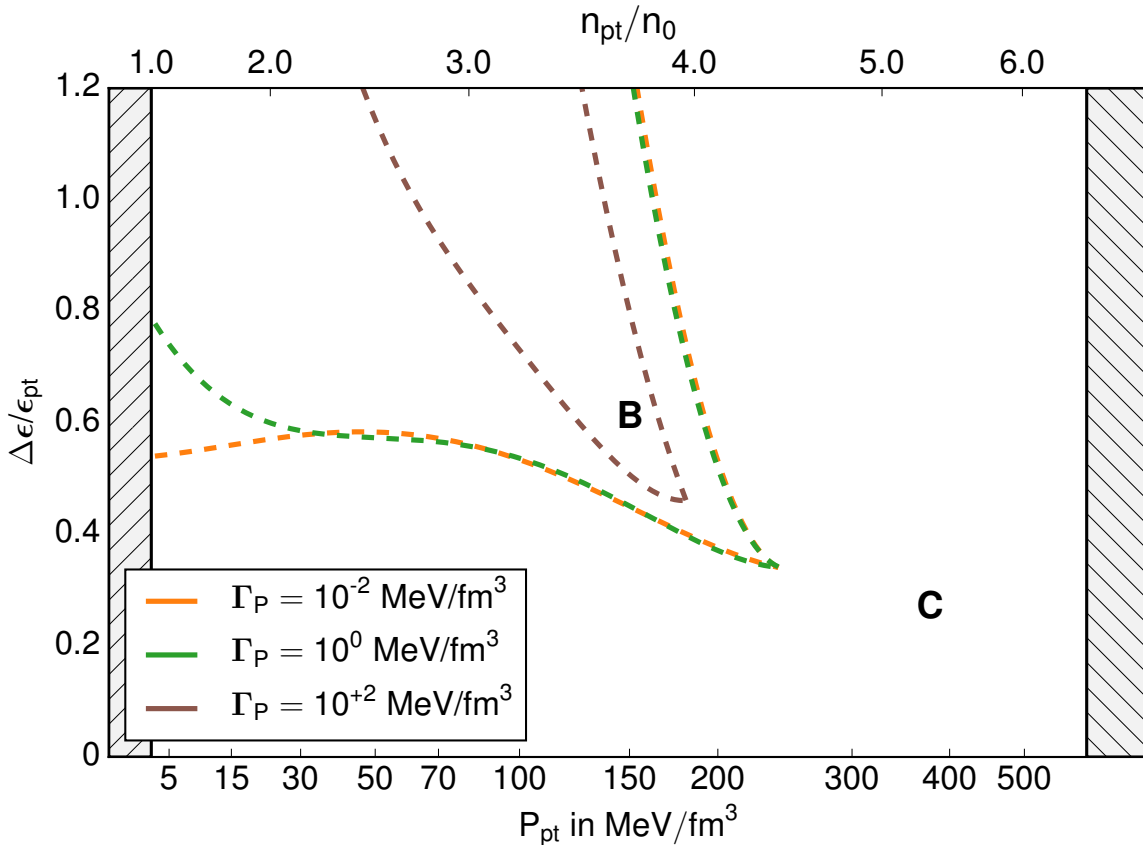

Figure 4.2: The "phase" diagram of the crossover parametrization for small values of the crossover region in comparison to the "phase" diagram of the CSS parametrization (blue line). The occurrence of the four MR curve types is visualized depending on the proportion $\Delta\epsilon/\epsilon_{pt}$ and P_{pt}. The BHF(N,l) EoS and $c_{QM}^2 = 1$ are used. The solid red line denotes the stabilization criterion (3.22). The shaded area at low densities ($n_{pt} < n_0$) is excluded since nuclear matter consists only of a hadronic phase. The hatched area at high densities is excluded because the transition pressure P_{pt} is above the central pressure of the heaviest pure hadronic star P_{max}.

In Figure 4.2 and 4.3 the "phase" diagrams for the crossover parametrization using various crossover regions Γ_P are visualized. In comparison the "phaselines" of the first-order phase transition are illustrated as well (blue lines) in Figure 4.2. Both parameterizations use the BHF(N,l) EoS and the quark matter sound velocity $c_{QM}^2 = 1$. Solid lines represent the border

between the regions with a connected branch (B and C) and those without a connected branch (A and D). Regions with a "third family" branch (B and D) are separated from other regions by dashed/dashed-dotted lines. As in the previous sections, the red solid line denotes criterion (3.22), the hatched area at low transition pressures ($n_{pt} < n_0$) is excluded because nuclear matter consists of a pure hadronic phase. The shaded area at high pressures is excluded, as the transition pressure P_{pt} is above the central pressure P_{max} of heaviest pure hadronic star and no stable hybrid stars could be found for even higher transition pressures.
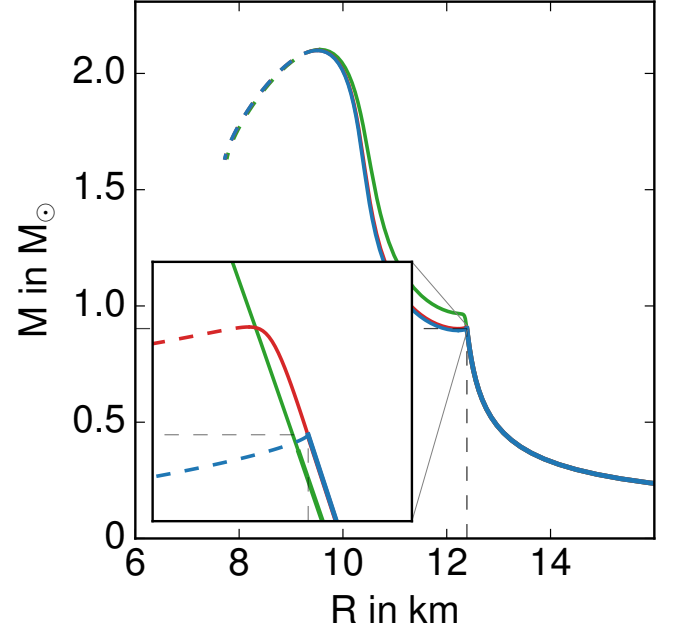
Since the limit of the crossover parametrization for negligible crossover regions ($\Gamma_P \to 0$) coincides with the first-order phase transition, it is understandable that the "phase" diagram for $\Gamma_P = 10^{-5}\,\mathrm{MeV/fm^3}$ is essentially equal to the CSS parametrization with $\Gamma_P = 0\,\mathrm{MeV/fm^3}$. The fluctuations of the solid lines of the crossover parametrization can be explained by numerical uncertainties and the lower resolution of the grid. With increasing but still very small crossover region ($\Gamma_P \ll 1\,\mathrm{MeV/fm^3}$, Figure 4.2), the "Both" region reaches to higher energy density discontinuities. The "phaselines" at high transition pressures and the settings for the occurrence of "third family" stars are nearly unchanged. All four MR types occur within the default limits of $\Delta\epsilon/\epsilon_{pt}$ and P_{pt}.

Figure 4.3: The "phase" diagram of the crossover parametrization for large values of the crossover region. The occurrence of the MR case B and C is visualized depending on the proportion $\Delta\epsilon/\epsilon_{pt}$ and P_{pt}. The BHF(N,l) EoS and $c_{QM}^2 = 1$ are used. The shaded area at low densities ($n_{pt} < n_0$) is excluded since nuclear matter consists only of a hadronic phase. The hatched area at high densities is excluded because the transition pressure P_{pt} is above the central pressure of the heaviest pure hadronic star P_{max}.

If we further increase the transition region (Figure 4.3), only regions with a connected branch occur. Even high transition pressures and energy density discontinuities will not destabilize neutron stars with a small percentage of quark matter inside the core. With increasing Γ_P the connected and disconnected branch of MR curves merge first at low transition pressures and then even at higher P_{pt}. Therefore region B is shrinking for $\Gamma_P \gtrsim 10^{-2}\,\mathrm{MeV/fm^3}$. At large crossover regions ($\Gamma_P = 100\,\mathrm{MeV/fm^3}$), "third family" stars can only occur for $50\,\mathrm{MeV/fm^3} \lesssim P_{pt} \lesssim 160\,\mathrm{MeV/fm^3}$ and large energy density discontinuities $\Delta\epsilon \gtrsim 350\,\mathrm{MeV/fm^3}$.

The development of the MR curve for fixed transition parameters $P_{pt}/\epsilon_{pt} = 0.08$ ($P_{pt} = 28.30\,\mathrm{MeV/fm^3}$), $\Delta\epsilon/\epsilon_{pt} = 0.72$ ($\Delta\epsilon = 264.65\,\mathrm{MeV/fm^3}$) and increasing Γ_P is shown in Figure 4.4. The transition settings correspond to region D for small crossover regions ($\Gamma_P = 10^{-4}\,\mathrm{MeV/fm^3}$). This case is indicated by the blue line. The star will be destabilized as soon as quark matter appears in the interior. For larger quark cores the star can balance the additional gravitational pull caused by the quark matter and stabilizes again. For increasing crossover region ($\Gamma_P = 1\,\mathrm{MeV/fm^3}$) the border between region D and B shifts to higher $\Delta\epsilon$ and the fixed transition parameters correspond to region B. The red line denotes this case and it is nearly identical to the previous "Disconnected" case except of the behavior directly after P_{pt}. The stars of the red line will not be destabilized immediately after the quark matter appears. For even larger crossover regions ($\Gamma_P \gtrsim 10\,\mathrm{MeV/fm^3}$), the "Connected" region reaches up to higher $\Delta\epsilon$ and contains the considered settings. For the green line, the connected and disconnected branch merged. The star will only be destabilized for large quark cores. Due to the fact, that a variation of Γ_P has a small influence on the the EoS even for $P < P_{pt}$, the slight shift of the green line to

Figure 4.4: MR curves using the crossover parametrization for fixed transition parameters $P_{pt}/\epsilon_{pt} = 0.08$, $\Delta\epsilon/\epsilon_{pt} = 0.72$ and different values of the crossover region Γ_P. The blue line indicates the "Disconnected" case for $\Gamma_P = 10^{-4}\,\mathrm{MeV/fm^3}$. With increasing crossover region ($\Gamma_P = 1\,\mathrm{MeV/fm^3}$) we will obtain the "Both" type which is visualized by the red line. For even higher crossover regions ($\Gamma_P = 10\,\mathrm{MeV/fm^3}$) the "Connected" case occurs (green line). Solid lines represent stable star configurations, dashed lines unstable ones.

lower radii at P_{pt} is explainable. For low or very high central pressures, the effects of the crossover parametrization are negligible and all three MR curves conform.

We will now focus on the physical background of the changes caused by using the crossover parametrization. In the CSS parametrization, the energy density has a jump discontinuity directly after the transition pressure. Therefore, the additional gravitational pull caused by the quark matter with increased energy density will rise abruptly. In contrast the energy density in the crossover parametrization will increase smoothly. Considering fixed P_{pt} and $\Delta\epsilon$, the gradient of ϵ inside the crossover region only depends on Γ_P. The larger Γ_P, the smaller is the gradient and therefore the increase of the gravitational pull, caused by the strong interacting matter in the crossover region. Hence stars with small percentages of quark matter tend to be more stable, if the crossover region increases. This effect is first noticeable at low transition pressures, because for low P_{pt} the hadronic mantle is not sufficiently massive to counteract even small additional gravitational pulls. If Γ_P is large, the percentage of the quark matter increases more slowly as a function of P_c. Therefore the percentage of hadronic matter is in general higher for a given central pressure and the star tends to be more stable. The larger Γ_P, the longer is the connected branch stable and the higher is the possibility to merge with a disconnected branch. Thus the region B is shrinking with increasing crossover region.

After we analyzed the changes of the "phase" diagram for various values of Γ_P, but fixed hadronic EoS and quark matter sound velocity, we examine changes of the "phase" diagram due to different hadron matter EoS and c_{QM}^2 in this section. For this reason we calculate the "phase" diagram for the χ SU(3) EoS, the sound velocity $c_{QM}^2 = 1/3$ and the same crossover regions as in Section 4.2. The "phase" diagram with these properties is shown in Figure 4.5 and 4.6. To compare the "phase" diagrams for low Γ_P with the "phase" diagram of the CSS parametrization, we visualize the "phaselines" of the first-order phase transition ($\Gamma_P = 0 \, \text{MeV/fm}^3$) as well.
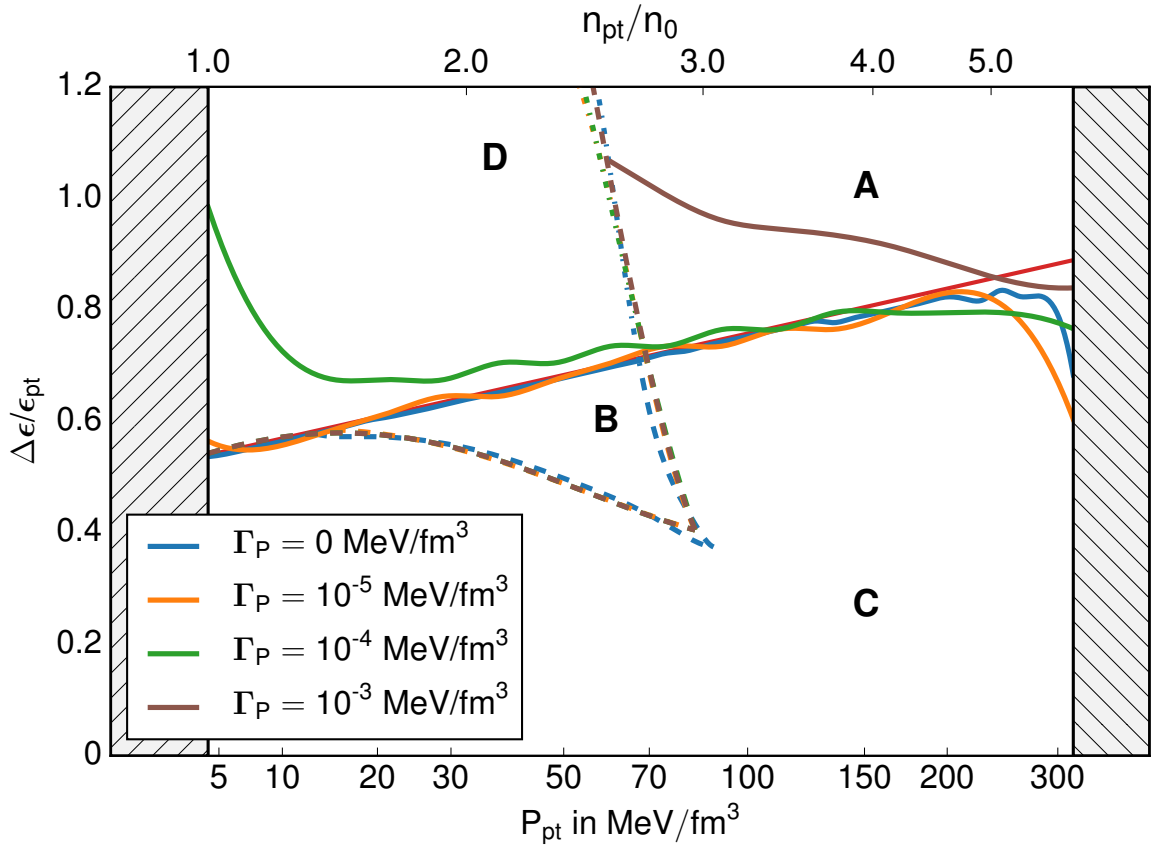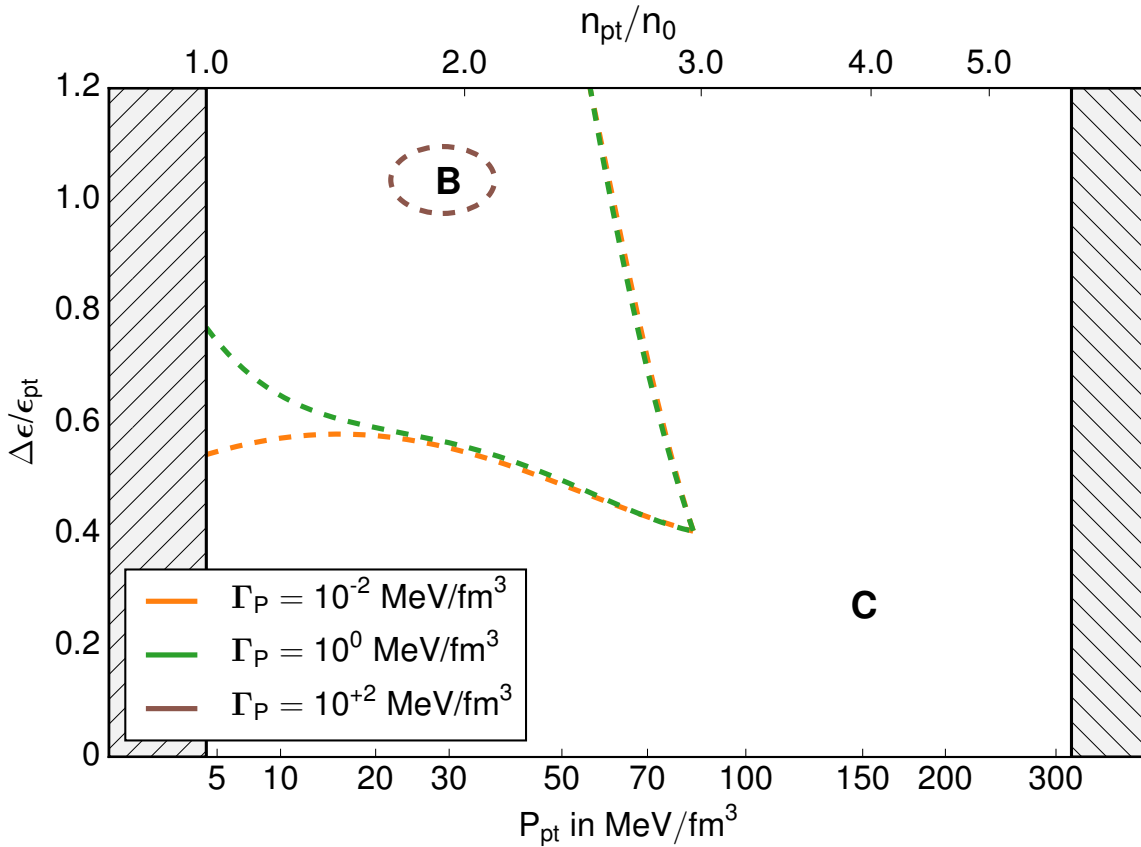

Figure 4.5: The "phase" diagram of the crossover parametrization for small values of the crossover region in comparison to the "phase" diagram of the CSS parametrization (blue line). The occurrence of the four MR curve types is visualized depending on the proportion $\Delta\epsilon/\epsilon_{pt}$ and P_{pt}. The χ SU(3) EoS and $c_{QM}^2 = 1/3$ are used. The solid red line denotes the stabilization criterion (3.22). The shaded area at low densities ($n_{pt} < n_0$) is excluded since nuclear matter consists only of a hadronic phase. The hatched area at high densities is excluded because the transition pressure P_{pt} is above the central pressure of the heaviest pure hadronic star P_{max}.

In general the "phaselines" of the new hadronic EoS and quark matter sound velocity behave analogously to the ones of Section 4.2. The dashed and dashed-dotted lines are nearly independent of the width of the crossover region for small Γ_P. For increasing Γ_P the solid lines move away from the line of criterion (3.22) and reach higher energy density discontinuities. This

process begins at low transition pressures. If we further increase Γ_P, regions with connected branches (B and C) reach up to very high energy density discontinuities and finally the region B starts to shrink.

Comparing the new "phaselines" with the ones in Section 4.2, we determine that the dashed/dashed-dotted line shifts to higher transition pressures for a larger sound velocity. This can be explained analogously to Section 3.3.3. With higher sound velocities, the pressure increases faster with the energy density. Hence "third family" stars with a quark matter core can sustain the massive hadronic mantle for even larger transition pressures. This shifts the dashed/dashed-dotted line to higher P_{pt}. In contrast to the BHF(N,l) EoS, the regions B and C of the χSU(3) EoS move faster to high energy density discontinuities as a function of Γ_P. For softer equations of state and fixed transition pressure, the transition energy density is higher and the hadronic mantle is more massive. Hence the hadronic mantle can counteract larger gravitational pulls of the strong interacting matter. The regions B and C can reach higher energy density discontinuities. Furthermore the area of region B becomes smaller for using softer EoSs at large Γ_P.

Figure 4.6: The "phase" diagram of the crossover parametrization for high values of the crossover region. The occurrence of the MR cases B and C is visualized depending on the proportion $\Delta\epsilon/\epsilon_{pt}$ and P_{pt}. The χSU(3) EoS and $c_{QM}^2 = 1/3$ are used. The shaded area at low densities ($n_{pt} < n_0$) is excluded since nuclear matter consists only of a hadronic phase. The hatched area at high densities is excluded because the transition pressure P_{pt} is above the central pressure of the heaviest pure hadronic star P_{max}.

5 Conclusion and outlook

In this thesis the general characteristics of the mass-radius curves of neutron stars were investigated. In this process we focused on the third stable branch of compact stars, the "third family" stars. It was topic of this work to analyze the occurrence and observables, like mass and radius of these stars, induced by a phase transition of first-order to a deconfined quark matter or a hadron-quark crossover.

At the beginning of this thesis, pure hadronic neutron stars were analyzed. We discussed their structure, derived the necessary equations to describe them mathematically and introduced the method of solving the Tolman-Oppenheimer-Volkoff equations. In this work we used the hadronic equations of state BHF(N,l) and χ SU(3). For these equations of states the mass-radius relations were calculated and discussed.

Since the appearance of deconfined quark matter is assumed to occur at high densities by the theory of QCD, we assumed a first-order phase transition at first. For the quark matter equation of state, a constant speed of sound approximation was used, which only depends on the sound velocity c_{QM}^2. The first-order phase transition to this quark matter equation of state was discussed and parametrized by the transition parameters P_{pt} (transition pressure) and $\Delta\epsilon$ (energy density discontinuity). Since a hybrid star with a small quark core is destabilized by a large discontinuity in energy density, a criterion was derived for this case to specify the critical value $\Delta\epsilon_{crit}$. Moreover we varied both transition parameters over a wide range and obtained four different types of mass-radius curves (A, B, C and D). The occurrence of the different regions of mass-radius types could be visualized in a "phase" diagram, which depended on P_{pt} and $\Delta\epsilon$. We obtained that for the occurrence of the two regions B and D, which contain "third family" stars, the phase transition must occur at low pressures and provide a large discontinuity in energy density. After that we investigated the dependency of the "phase" diagram on different hadronic EoS and c_{QM}^2. The maximal and minimal masses and radii of "third family" stars were shown by contour plots based on the "phase" diagram and were analyzed with respect to different EoSs. For the used EoSs the "third family" star masses ranged from $1.1\,M_\odot$ to $1.5\,M_\odot$. Since massive neutron stars with masses of $M \approx 2\,M_\odot$ could not be described by these EoSs, we concluded that the used EoSs are probably unrealistic. After that we analyzed the structure of a neutron star in comparison with its "third family" counterpart with the same mass and discussed why the observation of these "neutron star twins" gave a possible signature for a phase transition.

After we have shown that a first-order phase transition can lead to "third family" stars, we investigated if a smoother EoS could also lead to these stars. Therefore we introduced a hadron-quark crossover, which smoothed the sharp first-order phase transition as a function of the pressure transition region Γ_P. For this crossover we repeated the investigation of the occurrence of the four mass-radius types by using the "phase" diagram. We found out that even for sufficiently high $\Gamma_P \approx 100\,\mathrm{MeV/fm}^3$, "third family" stars can occur.

Since the mass and radius regions of "third family" stars partially overlap with the corresponding regions of neutron stars, it is not possible to distinguish between the two families with regard to mass or radius. Until now a reliable classification of "third family" stars is only possible by knowing the mass-radius curve or finding a "neutron star twin". Investigating other characteristics of "third family" stars could perhaps lead to a clear separation.

Even in theory, the "third family" stars and hybrid stars are not clearly separated. If the central densities of all possible "third family" stars are above the maximal limit of stable hybrid stars, this would lead to a well defined border between the two branches of compact stars.

As we can see in Figure 4.4, the smoothening of the phase transition leads to higher minimal masses of the third stable branch. As we have not analyzed the effects on mass and radius of "third family" stars by using a hadron-quark crossover, it would be interesting to do this in future work. This would give us the chance to locate the mass and radius regions of "third family" stars in case of a crossover phase transition.

Furthermore it would be interesting to know the effects on general characteristics of "third family" stars by using other approaches of the EoS. What happens if we use a third window method analogously to [5] or a first-order phase transition with a mixed phase (Gibbs construction)? In either case it would be surely interesting to know, if any other theory beside phase transitions and crossovers could lead to "third family" stars.

Bibliography

[1] K. Schertler et al. Quark phases in neutron stars and a "third family" of compact stars as a signature for phase transitions. *Nucl.Phys.*, A677:463–490, 2000.

[2] P. Haensel, A. Y. Potekhin, and D. G. Yakovlev. *Neutron stars 1: Equation of state and structure*, volume 326. Springer Science & Business Media, 2007.

[3] P. Demorest et al. Shapiro Delay Measurement of A Two Solar Mass Neutron Star. *Nature*, 467:1081–1083, 2010.

[4] J. Antoniadis et al. A Massive Pulsar in a Compact Relativistic Binary. *Science*, 340, 04 2013.

[5] T. Kojo et al. Phenomenological QCD equation of state for massive neutron stars. *Phys. Rev.*, D 91:045003, 12 2014.

[6] C. Sasaki. The QCD Phase Diagram from Chiral Approaches. *Nucl. Phys.*, A830:649C–656C, 2009.

[7] M. G. Alford, S. Han, and M. Prakash. Generic conditions for stable hybrid stars. *Phys. Rev.*, D 88:083013, 02 2013.

[8] M. A. Stephanov. Qcd phase diagram: an overview. *PoS LAT2006*, 024, 2006.

[9] K. Masuda, T. Hatsuda, and T. Takatsuka. Hadron-quark crossover and massive hybrid stars. *PTEP*, 2013(7):073D01, 2013.

[10] R. Kippenhahn and A. Weigert. *Stellar Structure and Evolution*. Springer Science & Business Media, 2012.

[11] S. L. Shapiro and S. A. Teukolsky. *Black holes, white dwarfs and neutron stars: the physics of compact objects*. John Wiley & Sons, 2008.

[12] N. K. Glendenning. *Compact stars: Nuclear physics, particle physics and general relativity*. Springer Science & Business Media, 2012.

[13] U. H. Gerlach. Equation of State at Supranuclear Densities and the Existence of a Third Family of Superdense Stars. *Phys. Rev.*, 172:1325–1330, 1968.

[14] B. K. Harrison et al. *Gravitation Theory and Gravitational Collapse*. University of Chicago Press, 1965.

[15] N. K. Glendenning and C. Kettner. Possible third family of compact stars more dense than neutron stars. *Astronomy and Astrophysics*, 353:L9–L12, January 2000.

[16] D. Page. Neutron Star: Surface and Interior, http://www.astroscu.unam.mx/neutrones /NS-Picture/NStar/NStar_l.gif. April 2017.

[17] J. M. Lattimer and M. Prakash. The Physics of Neutron Stars. *Science,* 304:536–542, 2004.

[18] A. Einstein. Die Feldgleichungen der Gravitation. *Sitzungsber. preuss. Akad. Wiss.,* 47.2:744–847, 1915.

[19] A. Einstein. Erklärung der Perihelbewegung des Merkur aus der allgemeinen Relativitätstheorie. *Sitzungsber. preuss. Akad. Wiss.,* 47.2:831–839, 1915.

[20] A. Einstein. Zur allgemeinen Relativitätstheorie. *Sitzungsber. preuss. Akad. Wiss.,* 47.2:799–801, 1915.

[21] T. Fließbach. *Allgemeine Relativitätstheorie.* Springer Science & Business Media, 2012.

[22] W. Nolting. *Grundkurs Theoretische Physik 4: Spezielle Relativitätstheorie, Thermodynamik.* Springer Science & Business Media, 2010.

[23] J. R. Oppenheimer and G. M. Volkoff. On Massive neutron cores. *Phys. Rev.,* 55:374–381, 1939.

[24] R. C. Tolman. Static Solutions of Einstein's Field Equations for Spheres of Fluid. *Phys. Rev.,* 55:364–373, February 1939.

[25] M. Camenzind. *Gravitation und Physik kompakter Objekte.* Springer Science & Business Media, 2014.

[26] C. E. Rhoades, Jr. and R. Ruffini. Maximum mass of a neutron star. *Phys. Rev. Lett.,* 32:324–327, 1974.

[27] W. Becker et al. *Neutron stars and pulsars.* Springer Science & Business Media, 2009.

[28] G. Baym, C. Pethick, and P. Sutherland. The Ground state of matter at high densities: Equation of state and stellar models. *Astrophys. J.,* 170:299–317, 1971.

[29] M. Baldo, I. Bombaci, and G. F. Burgio. Microscopic nuclear equation of state with three-body forces and neutron star structure. *Astron. Astrophys.,* 328:274–282, 1997.

[30] M. Hanauske et al. Neutron star properties in a chiral SU(3) model. *Astrophys. J.,* 537:958, 2000.

[31] P. Papazoglou et al. Chiral Lagrangian for strange hadronic matter. *Phys. Rev.,* C57:2576–2588, 1998.

[32] P. Papazoglou et al. Nuclei in a chiral SU(3) model. *Phys. Rev.,* C59:411–427, 1999.

[33] M. Buballa. NJL-model analysis of dense quark matter. *Phys.Rept.,* 407:205–376, 2005.

[34] F. Wegner. Vorlesungskriptum Theoretische Physik IV: Statistische Mechanik. Ruprecht-Karls-Universität Heidelberg, 2014.

[35] Y. Nambu and G. Jona-Lasinio. Dynamical Model of Elementary Particles Based on an Analogy with Superconductivity. 1. *Phys. Rev.,* 122:345–358, 1961.

[36] Y. Nambu and G. Jona-Lasinio. Dynamical Model of Elementary Particles Based on an Analogy with Superconductivity. 2. *Phys. Rev.,* 124:246–254, 1961.

[37] J. M. Weisberg, D. J. Nice, and J. H. Taylor. Timing Measurements of the Relativistic Binary Pulsar PSR B1913+16. *Astrophys. J.*, 722:1030–1034, 2010.

[38] S. E. Thorsett and D. Chakrabarty. Neutron star mass measurements. 1. Radio pulsars. *Astrophys. J.*, 512:288, 1999.

[39] Z. F. Seidov. The Stability of a Star with a Phase Change in General Relativity Theory. *Soviet Astronomy*, 15:347, 10 1971.

[40] B. Kämpfer. On stabilizing effects of relativity in cold spheric stars with a phase transition in the interior. *Phys. Rev. Lett.*, B101:366–368, 1981.

[41] J. L. Zdunik, P. Haensel, and R. Schaeffer. Phase transitions in stellar cores. II - Equilibrium configurations in general relativity. *Astronomy and Astrophysics (ISSN 0004-6361)*, 172:95–110, 1 1987.

[42] M. J. Lighthill. *Mon. Not. Roy. Astron. Soc.*, 110:339, 1950.

[43] M. G. Alford and Sophia Han. Characteristics of hybrid compact stars with a sharp hadron-quark interface. *Eur. Phys. J.*, A52(3):62, 2016.